J. Fluid Mech. (2003), *vol.* 489, *pp.* 155–184.
DOI: 10.1017/S0022112003005068 Printed in the United Kingdom

A model for deformable roll coating with negative gaps and incompressible compliant layers

By M. J. GOSTLING[1], M. D. SAVAGE[1], A. E. YOUNG[2] AND P. H. GASKELL[2]

[1]Department of Physics and Astronomy, The University of Leeds, Leeds LS2 9JT, UK

[2]School of Mechanical Engineering, The University of Leeds, Leeds LS2 9JT, UK

(Received 9 October 2000 and in revised form 3 March 2003)

A soft elastohydrodynamic lubrication model is formulated for deformable roll coating involving two contra-rotating rolls, one rigid and the other covered with a compliant layer. Included is a finite-strip model (FSM) for the deformation of the layer and a lubrication model with suitable boundary conditions for the motion of the fluid. The scope of the analysis is restricted to Newtonian fluids, linear elasticity/viscoelasticity and equal roll speeds, with application to the industrially relevant highly loaded or 'negative gap' regime. Predictions are presented for coated film thickness, inter-roll thickness, meniscus location, pressure and layer deformation as the control parameters – load (gap), elasticity, layer thickness and capillary number, Ca – are varied. There are four main results:

(i) Hookean spring models are shown to be unable to model effectively the deformation of a compliant layer when Poisson's ratio $\nu \to 0.5$. In particular, they fail to predict the swelling of the layer at the edge of the contact region which increases as $\nu \to 0.5$; they also fail to locate accurately the position of the meniscus, X_M, and to identify the presence, close to the meniscus, of a 'nib' (constriction in gap thickness) and associated magnification of the sub-ambient pressure loop.

(ii) Scaling arguments suggest that layer thickness and elasticity may have similar effects on the field variables. It is shown that for positive gaps this is true, whereas for negative gaps they have similar effects on the pressure profile and flow rate yet quite different effects on layer swelling (deformation at the edge of the contact region) and different effects on X_M.

(iii) For negative gaps and $Ca \sim O(1)$, the effect of varying either viscosity or speed and hence Ca is to significantly alter both the coating thickness and X_M. This is contrary to the case of fixed-gap rigid roll coating.

(iv) Comparison between theoretical predictions and experimental data shows quantitive agreement in the case of X_M and qualitive agreement for flow rate. It is shown that this difference in the latter case may be due to viscoelastic effects in the compliant layer.

1. Introduction

Industrial roll coating systems are relatively inexpensive to build and maintain, simple to operate and versatile, hence their continued widespread use for applying a thin liquid film onto a moving substrate in the form of a continuous reel of paper,

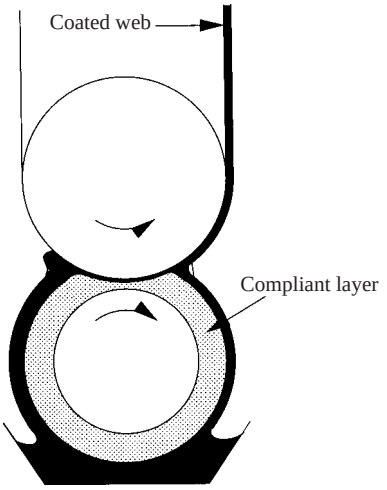

FIGURE 1. Cross-sectional schematic of a deformable roll coater operating in forward mode.

plastic or metal. Such systems can consist of a large number of paired rolls, each pair metering a continuous layer of liquid and operating in either forward (contra-rotating) or reverse (co-rotating) mode (Coyle 1997).

Despite their apparent complexity they can be analysed by understanding the flow between each roll pair in terms of film thickness ratio, roll separation and the ratios of the peripheral roll speeds and radii, see Benjamin & Scriven (1992). Roll pairs, for the case when both are rigid and separated by a small distance, or 'positive gap', have been studied exhaustively, both experimentally (Ho & Holland 1978; Benkreira, Edwards & Wilkinson 1981; Malone 1992; Decre, Gailly & Buchlin 1995; Gaskell, Innes & Savage 1998) and theoretically (Greener & Middleman 1975; Ruschak 1982, 1985; Coyle, Macosko & Scriven 1986, 1990*a*, *b*; Gaskell *et al.* 1995; Gaskell, Savage & Thompson 1998) and there remains little that is not known about the fluid mechanics that underpins them.

If one roll is rigid and the other is covered with a compliant layer a 'negative gap' is formed by nipping together the roll pair, see figure 1. This serves to: (i) minimize sensitivity to mechanical tolerances such as roll run-out and surface finish; (ii) avoid damage due to roll clash and the risk of wear; (iii) produce thinner films at higher production speeds and avoid or delay the onset of the ribbing instability (Carvalho & Scriven 1995*a*, 1997*a*, 1999). In practice the compliant layer is made from an elastomeric material which in general is incompressible. It is the analysis of this type of deformable roll coater, involving fluid–solid interactions (elastohydrodynamic lubrication), that forms the topic of this paper.

Elastohydrodynamic lubrication (EHL) has its origins in tribology with the work of Dowson & Higginson (1966). In 'soft EHL', where pressures are low and viscosity is assumed constant, Herrebrugh (1968), Hooke & O'Donoghue (1972) and Hall & Savage (1988*b*) investigated contacts in which the deformable bodies can be regarded as a half-space. The EHL of elastic layers was considered by Hooke (1986), Elsharkawy & Hamrock (1995) and Bohan *et al.* (1997). In every case the motion of the fluid was modelled by lubrication theory with Reynolds boundary conditions applied to terminate the flow regime. Since tribologists, unlike coating specialists,

are concerned with load carrying capacity rather than flow rate and film thickness prediction, Reynolds conditions prove sufficient and so it has not been necessary to consider different boundary conditions. Other references of interest are Houpert & Hamrock (1986), Jaffar (1990) and Xue, Gethin & Lim (1994, 1996).

When deformable bodies are in dry contact, displacement and contact pressure are related via an integral equation. This equation expresses the fact that pressure, at every point of the contact, contributes to the displacement at a given point. A Chebyshev series method was developed by Hall & Savage (1988*a*) for dry contact problems and subsequently applied to elastohydrodynamic contacts (Hall & Savage 1988*b*). This series method was extended to contacts with deformable layers by Jaffar & Savage (1988), and Myers, Savage & Gaskell (1994).

Research into deformable roll coating began with the pioneering work of Coyle (1988) who presented a simple analysis based on lubrication theory and Reynolds conditions for the fluid coupled with a one-dimensional constrained column model (CCM) (which it should be noted is invalid in the context of incompressible materials) for the deformation of the compliant layer. Essentially the latter is a simple Hookean spring model in which the local fluid pressure is assumed to be directly proportional to the local deformation. In doing so he was the first to attempt to predict the variation in resultant film thickness for both positive- and negative-gap regimes. Recent experimental results (Cohu & Magnin 1995, 1997) highlight the effect of the depth of the compliant layer on the resultant film thickness, indicating agreement with Coyle's theory for thick layers only. Indeed, they show that decreasing the elastomer covering below a critical value tends to decrease the coating thickness significantly.

Carvalho and Scriven attempted to validate the CCM used by Coyle by proposing and comparing several distinct models for the deformation of a compliant layer coupled with a fluid model for fully submerged rolls, i.e. no free surfaces present. First, they considered (Carvalho & Scriven 1994): (i) a one-dimensional Hookean spring model; (ii) a one-dimensional neo-Hookean model; (iii) a two-dimensional linear elasticity model for which the deformable layer is regarded as an infinite half-space (HSM) – the other physical extreme to the CCM. Their results revealed that flow rate predictions obtained with each model differed by less than 10%. However, these results should be treated with a degree of caution as the effect of layer thickness was not explored and the HSM is only valid for deep layers. Secondly, they compared (Carvalho & Scriven 1997*b*) the CCM to a model that treated the elastomer as a Mooney–Rivlin material. They produced results that highlighted the effects of gap setting, elasticity and layer thickness on flow rate and found that, by varying the constant of proportionality inherent in the CCM, good agreement between the two models could be achieved. However, the constant of proportionality was assumed to be a multiple of E/L, where E is Young's modulus and L is the thickness of the compliant layer, and therefore there is an implicit assumption that E and L^{-1} have the same effect on the field variables. Also, free-surface effects were discarded during the comparisons and consequently their results do not fully justify the use of such a calibrated CCM in the general case. In addition, the CCM is incapable of preserving the deformable layers' volume – a prerequesite for incompressible materials.

Despite the weaknesses associated with any calibrated version of the CCM, it has been used to perform both steady-state investigations (Carvalho & Scriven 1995*b*, 1996) and linear stability analyses (Carvalho & Scriven 1997*a*, 1999) of the deformable roll coating process in the presence of a free surface. With the use of the CCM these

results indicate that deformable roll coating is a more stable process than its rigid roll counterpart. The effect of capillary number has been investigated (Carvalho & Scriven 1996) in the positive-gap regime and it was shown to have a similar affect on the field variables as in fixed-gap rigid roll coating. However, the effects in the industrially relevant negative-gap regime were not explored.

Predictions of these elastic models differ substantially from experimental results (Cohu & Magnin 1997) and this led to investigations of the viscoelastic effects in the compliant layer. Carvalho & Scriven (1996) used a modified CCM and Carvalho (1999) used a two-dimensional plane-strain model, along with a fully flooded fluid model, and in each case it was shown that the inclusion of viscoelastic effects led to a significant change in the flow rate predictions. In the present paper the affect of viscoelastic properties on the flow rate as well as the meniscus position are reported.

It is clear that the work of Carvalho and Scriven has contributed substantially to our knowledge and understanding of deformable roll coating. This has been achieved by employing a range of (i) elastomer deformation models – from simple Hookean spring models to those incorporating plane-strain nonlinear viscoelastic constitutive equations and (ii) fluid models and boundary conditions. Nevertheless in the industrially relevant case of incompressible layers (Poisson's ratio $\nu = 0.5$) and negative gaps certain key questions remain open. These are as follows:

1. How effective are Hookean spring models in modelling elastomer deformations as $\nu \to 0.5$?

2. What are the effects of layer thickness L and elasticity E on the field variables? Scaling arguments suggest that L and E^{-1} should cause similar effects – but is this true?

3. What is the effect of varying capillary number on flow rate and meniscus location in the negative gap regime?

4. What are the possible explanations for the difference between theory and experiment?

The aim of this paper, therefore, is to address the above questions by employing a finite-strip model (FSM) for the deformation of the compliant layer and a lubrication model with suitable boundary conditions for the motion of the fluid. Answers to these questions are essential to achieving a full understanding of the equilibrium deformable roll coating problem. In turn this is a necessary prerequisite for gaining full insight into the problem of instabilities.

2. Formulation of a mathematical model

2.1. *Modes of operation and governing parameters*

A deformable roll pair may be operated in one of two modes: fixed gap or fixed load. In the former, roll separation, $2H_0$, is set by the adjustment of mechanical stops, while in the latter it is achieved by varying an external force, W, applied across the roll pair.

In fixed-gap operation W is the roll separating force, which is a dependent variable, whereas for fixed-load operation H_0 is a dependent variable. In addition, roll separation may be set either at a positive gap where the centre to centre distance is greater than the sum of the roll radii, or at a negative gap where the rolls would be in interference if undeformed – as illustrated in figure 2.

Deformable roll coating devices are most commonly operated in a fixed-load, negative-gap regime. However, following Coyle (1988), it is more convenient to

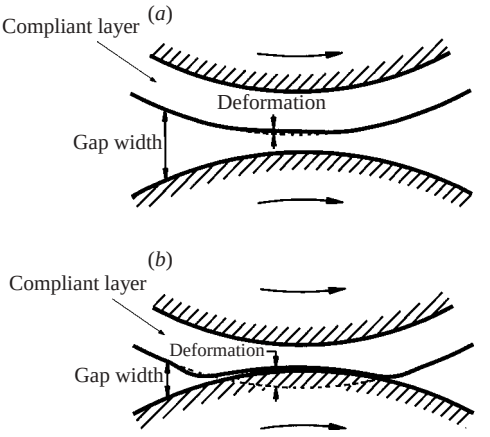

FIGURE 2. Schematics of the contact region showing (*a*) the positive- and (*b*) negative-gap regimes of operation. The undeformed roll profile is also shown (- -).

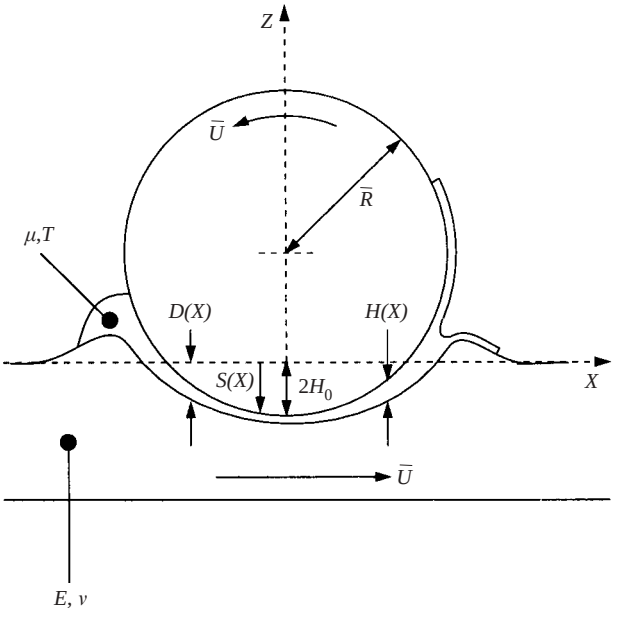

FIGURE 3. The geometry and physical parameters of the coating device.

formulate the deformable roll coating model based on a fixed-gap regime, and to calculate the equivalent roll separating force *a posteriori*. The roll pair geometry is approximated by a rigid roll and a compliant strip as shown in figure 3, which indicates the gap thickness $H(X)$ and surface deformation $D(X)$. The effective roll radius, $\bar{R}$, is set via $2/\bar{R} = 1/R_1 + 1/R_2$, where R_1 and R_2 are the radii of the original roll pair, thus preserving the gap width in the contact region at leading order.

Fluid–solid interaction is the key feature of a deformable roll pair, and the competition between viscous force, elastic force, and external or roll separating force may be represented by several dimensionless groups. For fixed-load operation, the

coated film thickness, H^∞, is controlled by varying the load parameter

$$F = \frac{W}{E\bar{R}}, \tag{2.1}$$

equal to the ratio of external force to an elastic force. For fixed-gap operation, H^∞ is controlled by varying the gap parameter

$$\frac{H_0}{\bar{R}}. \tag{2.2}$$

A non-dimensional elasticity number is defined by

$$E_S = \frac{\mu\bar{U}}{E\bar{R}}, \tag{2.3}$$

where μ is the fluid viscosity, and $\bar{U}$ is the roll speed. The ratio of viscous to surface tension forces at the downstream meniscus is represented by the capillary number

$$Ca = \frac{\mu\bar{U}}{T}, \tag{2.4}$$

where T is the surface tension at the fluid/air interface.

The ratio of compliant layer thickness to average roll radius, $L/\bar{R}$, is another important parameter, especially if L is comparable with the width of the contact, A, where typically $A/L \in [0.1, 1]$ for coating applications. To aid classification of the contact geometry, a dimensionless *strip number* can be identified as

$$\alpha = \frac{L}{A^*} = \frac{L}{\bar{R}}\left(\frac{H_0}{\bar{R}}\right)^{-1/2}, \tag{2.5}$$

in which $A^* = (\bar{R}H_0)^{1/2}$ is referred to as the *nominal contact width*. When $\alpha \gg 1$ the compliant layer is well-represented by an infinite half-space, and the contact is considered Hertzian. Under these conditions the contact width is less than A^*, since the compliant layer recedes (as opposed to swells) at the contact edge, as shown in figure 4(*a*). If $\alpha \ll 1$, then thin-strip theory is applicable, enabling the deformation of the layer to be described via a local deformation model for which the deformation at a point X depends only on the local pressure, $P(X)$. Under these conditions the contact width exceeds A^*, since the compliant layer swells at the contact edge due to the incompressibility, as shown in figure 4(*b*). Finally, for $\alpha = O(1)$ a finite-strip model (FSM) is required, such as that formulated for elastic layers by Bentall & Johnson (1968).

Compressibility of the compliant layer is represented by Poission's ratio, ν, and in the industrially relevant case of incompressible layers $\nu = 0.5$. The range of the independent parameters considered is summarized in table 1.

2.2. *Governing equations for thin-film fluid flow*

When the effective roll radius, $\bar{R}$, is large compared to the roll separation, H_0, $(H_0/\bar{R} \ll 1)$ lubrication theory can be used to model the fluid flow in the thin separating film. This gives rise to Reynolds equation, relating hydrodynamic pressure, $P(X)$, to the inter-roll film thickness, $H(X)$:

$$\frac{\mathrm{d}}{\mathrm{d}X}\left[\frac{H^3(X)}{\mu\bar{U}}\frac{\mathrm{d}P}{\mathrm{d}X}\right] = 12\frac{\mathrm{d}H}{\mathrm{d}X}, \tag{2.6}$$

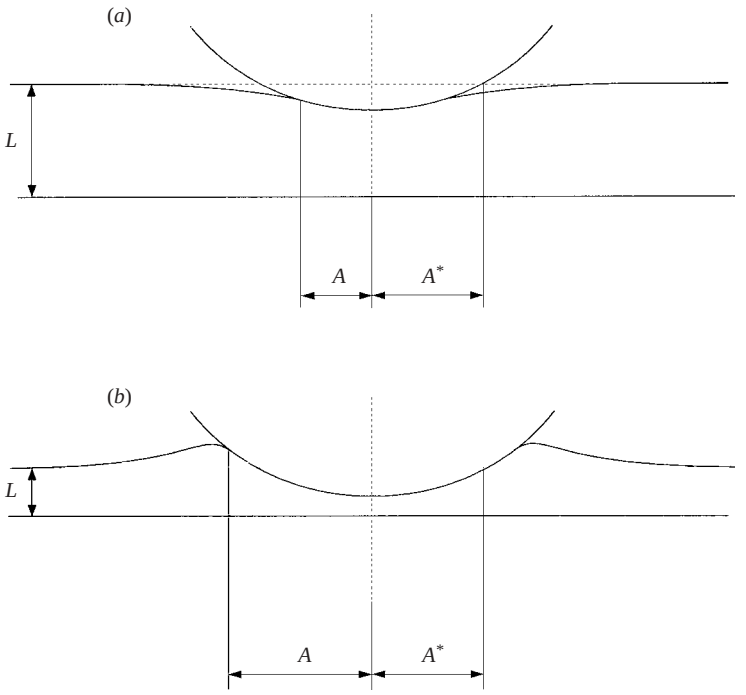

FIGURE 4. (*a*) Thick-strip, $A < A^*$, and (*b*) thin-strip, $A > A^*$, regimes.

Parameter	Range
$H_0/\bar{R}$	$[-10^{-2}, 10^{-2}]$
Ca	$[0.5, 2]$
E_S	$[10^{-7}, 10^{-5}]$
$L/\bar{R}$	$[0.05, 0.2]$

TABLE 1. The parameter range considered here. $E_S = 0$ is treated as a special case.

or in integrated form for iso-viscous flows:

$$\frac{\mathrm{d}P}{\mathrm{d}X} = 12\mu\bar{U}\left[\frac{H(X) - 2H^{\infty}}{H^3(X)}\right]. \tag{2.7}$$

$H(X)$ is expressed as the sum of the undeformed roll separation, $S(X)$, and the deformation of the layer, $D(X)$:

$$H(X) = S(X) + D(X), \tag{2.8a}$$

$$S(X) = 2H_0 + \frac{X^2}{\bar{R}}, \tag{2.8b}$$

where the parabolic approximation is used for the roll separation and H_0 is less/greater than zero for negative/positive gaps. Note that $Z = -D(X)$ and $Z = S(X)$ represent the surfaces of the compliant layer and rigid roll respectively. This approximation is valid to $O(H_0/\bar{R})$ where $2H_0$ is the roll separation for positive gaps, and interference for negative gaps.

In lubrication theory, the dimension of the fluid domain is reduced by one and the position of the downstream meniscus is unknown *a priori*. Suitable boundary conditions to locate the extrema of the fluid domain are described below.

Boundary conditions

At the meniscus, X_M, the radius of curvature, $\mathscr{R}$, is given by means of an arc-of-circle approximation,

$$\mathscr{R} \approx \tfrac{1}{2}[H(X_M) - 2H^\infty], \tag{2.9}$$

and fluid pressure is taken to be capillary pressure such that

$$P(X_M) = -\frac{2T}{H(X_M)(1-2\beta)}, \tag{2.10}$$

where

$$\beta = \frac{H^\infty}{H(X_M)}. \tag{2.11}$$

With a fully flooded inlet region, fluid pressure far upstream of the nip is assumed to be ambient,

$$P(-\infty) = 0. \tag{2.12}$$

One additional boundary condition is then required to close the problem and its form is dependent on the value of Ca. For small capillary numbers, $Ca < 10^{-2}$, as for example in meniscus coating (Gaskell *et al.* 1995), the Landau & Levich (1942) expression relates H^∞ to $\mathscr{R}$, the radius of curvature of the meniscus,

$$\frac{H^\infty}{\mathscr{R}} = 1.34Ca^{2/3}, \tag{2.13}$$

which, in turn, gives a condition on the pressure gradient. In deformable roll coating however, capillary numbers are much larger and usually in excess of unity. In this range of Ca there is only one stagnation point downstream of the nip which is attached to the meniscus (Gaskell *et al.* 1998). For equal speeds it is located by the Prandtl (1904)–Hopkins (1957) (PH) conditions:

$$U = \frac{\partial U}{\partial Z} = 0 \qquad \text{at} \qquad (X, Z) = (X_M, -D(X_M) + H(X_M)/2), \tag{2.14}$$

which gives

$$\beta = \tfrac{1}{6}, \tag{2.15}$$

and the following condition on pressure gradient:

$$\left.\frac{\mathrm{d}P}{\mathrm{d}X}\right|_{X_M} = \frac{8\mu\bar{U}}{H^2(X_M)}. \tag{2.16}$$

In the case of unequal roll speeds symmetry arguments no longer apply and a two-dimensional flow analysis is needed to locate the stagnation point.

2.3. *Governing equations for the compliant layer*

The compliant layer is described by the Maxwell–Thomson model (Goryacheva 1998) which allows the inclusion of linear viscoelastic effects. The constitutive equations

linking the strain, ϵ^0_{ij}, and the stress, σ^0_{ij}, take the form

$$\epsilon^0_{X^0X^0} + T_\epsilon \frac{\partial \epsilon^0_{X^0X^0}}{\partial T} = \frac{1-\nu^2}{E}\left(\sigma^0_{X^0X^0} + T_\sigma \frac{\partial \sigma^0_{X^0X^0}}{\partial T}\right) - \frac{\nu(1+\nu)}{E}\left(\sigma^0_{Y^0Y^0} + T_\sigma \frac{\partial \sigma^0_{Y^0Y^0}}{\partial T}\right), \quad (2.17)$$

$$\epsilon^0_{Y^0Y^0} + T_\epsilon \frac{\partial \epsilon^0_{Y^0Y^0}}{\partial T} = \frac{1-\nu^2}{E}\left(\sigma^0_{Y^0Y^0} + T_\sigma \frac{\partial \sigma^0_{Y^0Y^0}}{\partial T}\right) - \frac{\nu(1+\nu)}{E}\left(\sigma^0_{X^0X^0} + T_\sigma \frac{\partial \sigma^0_{X^0X^0}}{\partial T}\right), \quad (2.18)$$

$$\epsilon^0_{X^0Y^0} + T_\epsilon \frac{\partial \epsilon^0_{X^0Y^0}}{\partial T} = \frac{1+\nu}{E}\left(\sigma^0_{X^0Y^0} + T_\sigma \frac{\partial \sigma^0_{X^0Y^0}}{\partial T}\right), \quad (2.19)$$

where T_ϵ is a retardation time and T_σ is a relaxation time. Two non-dimensional quantities can be defined: the Deborah number

$$De = \frac{T_\epsilon \bar{U}}{\sqrt{\bar{R}H_0}}, \quad (2.20)$$

which represents the ratio of the retardation time to a typical timescale of the flow; and

$$\frac{T_\epsilon}{T_\sigma}, \quad (2.21)$$

the ratio of the two viscoelastic timescales. The inclusion of the strain rate and stress rate terms allows the modelling of simple linear viscoelastic effects, whereas setting these two timescales equal to zero recovers the plane-strain linear elasticity equations. The coordinates (X^0, Y^0) represent a material frame of reference that is related to the laboratory frame, in which the axis of the roll is fixed and the deformation and pressure profiles are steady, via

$$X = X^0 + \bar{U}T, \qquad Y = Y^0. \quad (2.22)$$

Making the transformation

$$\epsilon^0_{ij} + T_\epsilon \frac{\partial \epsilon^0_{ij}}{\partial T} = \epsilon^0_{ij} + T_\epsilon \bar{U} \frac{\partial \epsilon^0_{ij}}{\partial X} = \epsilon^*_{ij}, \quad (2.23)$$

$$\sigma^0_{ij} + T_\sigma \frac{\partial \sigma^0_{ij}}{\partial T} = \sigma^0_{ij} + T_\sigma \bar{U} \frac{\partial \sigma^0_{ij}}{\partial X} = \sigma^*_{ij}, \quad (2.24)$$

$$U_S + T_\epsilon \bar{U} \frac{\partial U_S}{\partial X} = U^*_S, \qquad V_S + T_\epsilon \bar{U} \frac{\partial V_S}{\partial X} = V^*_S, \quad (2.25)$$

where U_S and V_S are the displacements in the X- and Y-directions, produces the variables ϵ^*_{ij} and σ^*_{ij} that satisfy the equations of an isotropic linear elastic material. These equations can be solved by the method of Fourier transforms (Bentall & Johnson 1968) and in the general case, the deformation at any position on the surface of the compliant layer is influenced by the entire normal surface stress distribution, $P(X)$, and this is expressed via an integral equation:

$$D^*(X) = \frac{(1-\nu^2)}{\pi E} \mathrm{Re} \int_{-\infty}^{\infty} \tilde{K}(\omega)(1 + \mathrm{i}\omega T_\sigma \bar{U}) \tilde{P}(\omega) \mathrm{e}^{\mathrm{i}\omega X/L} \, \mathrm{d}\omega, \quad (2.26)$$

where $\tilde{P}$ is the Fourier transform of P,

$$\tilde{K}(\omega) = \frac{(3-4\nu)\sinh 2\omega - 2\omega}{2\omega(\omega^2 + (1-2\nu)^2 + (3-4\nu)\cosh^2\omega)} \tag{2.27}$$

and the deformation, $D(X)$, is given by

$$D(X) = \frac{1}{T_\epsilon \bar{U}} \int_{-\infty}^{X} D^*(S)\exp((S-X)/T_\epsilon \bar{U})\,\mathrm{d}S. \tag{2.28}$$

The equivalent integral equation for purely elastic layers was given by Aleksandrov (1962), and used by Meijers (1968) for the dry contact of a rigid cylinder on an elastic strip bonded to a rigid undeformable backing. Contributions to the deformation from the tangential traction forces have been discarded as they are $O((H_0/\bar{R})^{3/2})$ and $O((H_0/\bar{R})^{-3/2}E_S^{3/2})$ in comparison to the normal forces in positive and negative gaps, respectively. This completes the description of the finite-strip deformation model (FSM).

In previous research, much simpler deformation models have been used to describe the behaviour of the compliant layer by relating the local deformation to the local pressure. These are referred to as local deformation models. The *constrained column model* (CCM) is derived from Hooke's law, with $D(X)$ given by

$$D(X) = P(X)/K, \quad K = \frac{(1-\nu)}{(1+\nu)(1-2\nu)}\frac{E}{L}, \tag{2.29}$$

where the constant of proportionality is often referred to as a *spring stiffness*, K.

Clearly, the CCM is restricted to compressible layers for which $\nu < 0.5$. For incompressible thin strips Meijers (1968), and Bentall & Johnson (1968) formulated the *incompressible strip model* (ICM) which yields the relationship

$$D(X) = -\frac{L^3}{E}\frac{\partial^2 P}{\partial X^2}. \tag{2.30}$$

These local deformation models (CCM and ICM) are assessed relative to the FSM for both dry and lubricated contacts in § 3.

2.4. *Numerical methods*

A brief summary only of the solution method is given below while the reader is referred to Young (1997) and Gostling (2002) for a more detailed account.

A finite element (FE) formulation is used to discretize and solve the EHL equations. As with any FE analysis, the solution domain is divided into a number of elements with the field variables, $P(X)$ and $D(X)$, represented in element e via a finite number of nodal freedoms, P_{e_i} and D_{e_i}, defined at nodal locations, X_{e_i}. The field variables are approximated with second-order polynomial interpolation functions and hence each element contains three nodes (interpolation points), typically located at each endpoint and the midpoint of the element. For element e, the node locations are X_{e_1}, X_{e_2} and X_{e_3} with related nodal unknowns P_{e_1}, P_{e_2} and P_{e_3} and D_{e_1}, D_{e_2} and D_{e_3}.

The aim is to substitute the approximations into the governing equations and vary the nodal unknowns until some measure of the error is minimized. Substitution into (2.6) is straightforward but (2.26) presents two problems. First, the integrand contains the Fourier transform of the pressure and so the transform of the pressure

approximation is required:

$$\tilde{P}(\omega) \approx -\frac{L}{\mathrm{i}\omega}\exp(-\mathrm{i}\omega X_M/L)P(X_M) + \frac{L^2}{\omega^2}\sum_{e=1}^{N}\left[2a_{e_2}\left[x_{e_2}\exp\left(-\mathrm{i}\omega X_{e_2}/L\right)\right.\right.$$
$$-x_{e_1}\exp\left(-\mathrm{i}\omega X_{e_1}/L\right) + \frac{L}{\mathrm{i}\omega}\exp\left(-\mathrm{i}\omega X_{e_2}/L\right) - \frac{L}{\mathrm{i}\omega}\exp\left(-\mathrm{i}\omega X_{e_1}/L\right)\Big]$$
$$\left.+a_{e_1}\left[\exp\left(-\mathrm{i}\omega X_{e_2}/L\right) - \exp\left(-\mathrm{i}\omega X_{e_1}/L\right)\right]\right], \tag{2.31}$$

where a_{e_1} and a_{e_2} are defined as

$$a_{e_1} = \frac{-3\lambda_e P_{e_1} + 4\lambda_e P_{e_2} - \lambda_e P_{e_3} - 4P_{e_1}X_{e_1} + 8P_{e_2}X_{e_1} - 4P_{e_3}X_{e_1}}{\lambda_e^2}, \tag{2.32}$$

$$a_{e_2} = 2\frac{P_{e_1} - 2P_{e_2} + P_{e_3}}{\lambda_e^2} \quad \text{and} \quad \lambda_e = X_{e_3} - X_{e_1}. \tag{2.33}$$

Secondly, (2.26) contains D^*, and so an intermediate set of nodal unkowns is introduced, D_i^*, linked to the deformation nodal unknowns, D_i, via (2.28). For each nodal freedom there is a corresponding field equation, conditions (2.12) and (2.16) are incorporated as natural boundary conditions and (2.10) completes the system. The upstream boundary condition, (2.12), is applied at a sufficently large negative value of X, chosen such that moving this point further upstream has a negligible effect on the solution. The nodal locations, X_i, are parameterized by X_M and this allows all the unknown variables to be determined simultaneously in a single iterative loop, which greatly improves the convergence characteristics of the solution method – referred to as a *total-Jacobian* iterative method. Local mesh refinement is used to improve the discrete representation of $P(X)$ local to X_M, whilst keeping the size of the numerical problem manageable.

The resulting residual equations for this highly nonlinear problem, written as $\boldsymbol{R}(\boldsymbol{X}) = \boldsymbol{0}$ with $\boldsymbol{X} = (P_1, P_2, \ldots, D_1, D_2, \ldots, X_M)$, were solved via Newton iteration, for the range of parameters shown in table 1, using zeroth-order continuation to move smoothly through parameter space.

Other important features of the method of solution are: (i) a fixed-gap problem with H_0 imposed rather than a fixed-load problem is solved; (ii) an analytic rigid roll solution was used as an initial guess to obtain results in the positive-gap regime followed by continuation through to negative gaps; (iii) the dimensional, rather than dimensionless, form of the equations was solved as this enabled the solution to move smoothly from the positive- to negative-gap regime.

3. Assessment of the local deformation models

The aim here is to assess the suitability of the local deformation models, CCM and ICM, for representing the deformation of a thin and incompressible elastic layer. The assessment is made by comparing predictions for contact-width, pressure and deformation distributions to those predicted by the FSM for both dry and lubricated conditions. The effect of incompressibility is investigated by considering the behaviour of the elastomer as $\nu \to 0.5$.

3.1. *Dry contacts: an equivalent contact*

The dry contact problem of a rigid cylindrical indentor on a flat bonded strip is solved using each of the three deformation models. The deformation, $D(X)$, inside

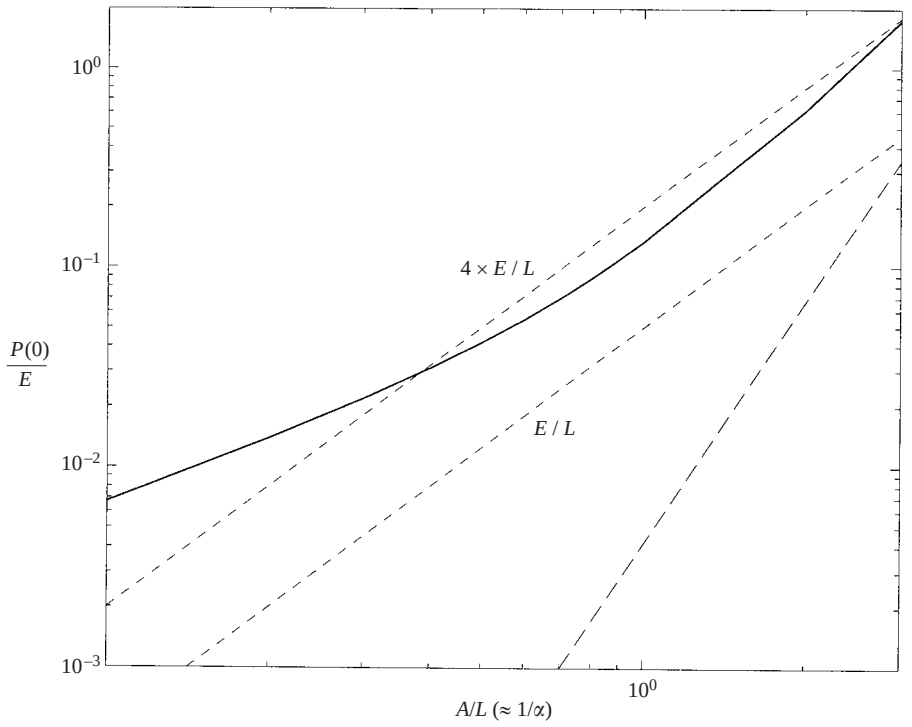

FIGURE 5. The variation of centreline pressure, $P(0)/E$, with A/L for the FSM (—), ICM (– –), and CCM (- -). Results are shown for the CCM with both $K' = E/L$ and $K' = 4 \times E/L$. $L/\bar{R} = 0.1$, $\nu = 0.5$.

the contact is imposed using the parabolic approximation to a circle, and the normal surface traction, $P(X)$, outside the contact is set to zero, thus

$$\begin{aligned} D(X) &= D_0 - X^2/\bar{R} \quad \text{for } |X| < A, \\ P(X) &= 0 \qquad\qquad\quad \text{for } |X| \geqslant A. \end{aligned}$$

In the classical contact problem, either the load or the centreline indentation, D_0, is imposed. This gives an inverse problem, as the contact width is not known *a priori*. Since the purpose of this exercise is to compare the deformation models, a simpler problem is therefore solved in which A/L is imposed and D_0 is subsequently calculated. For given values of ν and $L/\bar{R}$, the three deformation models are used to determine $P(X)$ inside the contact. Inspection of (2.29) however reveals that when $\nu = 0.5$ no deformation of the layer is predicted, regardless of the pressure distribution, and hence the CCM is invalid for incompressible materials. In fact work by Meijers (1968) and Jin & Dowson (1989) has shown that the CCM gives accurate results only for thin layers of compressible material with $\nu < 0.4$ and $A/L > 2$. Coyle (1988) and Carvalho & Scriven (1994) attempted to overcome this inherent limitation of the CCM by replacing the definition of K found in (2.29) with an effective stiffness, $K' = E/L$, which essentially corresponds to $\nu = 0$. Numerical solutions of the FSM were generated for $P(0)$ in the range $A/L \in [0.1, 10]$, with $L/\bar{R} = 0.1$ and $\nu = 0.5$ and compared with results via the ICM and CCM as shown in figure 5. Whatever the value of K the CCM fails to represent the lateral strain and under-predicts $P(0)$ (see figure 5). Carvalho & Scriven (1995*b*) made an attempt to improve the quantitative agreement of their spring model at $\nu = 0.5$ by introducing $K' = 4 \times E/L$, which

does give closer agreement with the FSM near $\alpha = 1$, as seen in figure 5. More recently, Carvalho & Scriven (1997*b*) have suggested a further modification to the spring constant, $K' = 2 \times E/L$; yet clearly no amount of *ad hoc* modification of the stiffness can mask the fact that the CCM is strictly invalid for incompressible materials which require the conservation of volume to be taken into account.

The ICM is a thin-strip model, derived for application to incompressible layers, and as such one would expect it to be valid as $\alpha \to 0$. Unfortunately, figure 5 shows that acceptable agreement is not achieved within the range of realistic operating conditions. Hence, the ICM is deemed unsuitable for modelling the deformation of compliant layers in deformable roll coating.

3.2. *Lubricated contacts*

Here the CCM and the FSM are assessed in the soft EHL regime, figures 6 and 8, where the appropriate non-dimensional variables are

$$x = \frac{X}{L}, \quad p(x) = \frac{P(X)}{E}\left(\frac{L}{H_0}\right), \quad d(x) = \frac{D(X)}{H_0}, \quad h(x) = \frac{H(X)}{L}$$

A solution of the soft EHL equations for pressure, $p(x)$, and gap thickness, $h(x)$, for both the CCM and FSM are compared in figure 6 for the parameter set: $Ca = 1$; $E_S = 10^{-5}$; $H_0/\bar{R} = -10^{-2}$; $L/\bar{R} = 10^{-1}$ ($\alpha = 1$); and $\nu = 0$ ($K' = E/L$). As expected, results for the two models are in close agreement. Nevertheless, there is one important distinguishing feature, namely the presence of a nib (constriction of gap thickness) or constriction of $h(x)$ close to x_m. This feature, well known in EHL studies (Hooke 1986), is not predicted by the CCM and therefore close to x_m the corresponding pressure curve is less steep and the ambient pressure loop is of smaller magnitude.

Differences in predictions between the FSM and various Hookean models (CCM) become more apparent as $\nu \to 0.5$. These are seen by using non-dimensional variables $\hat{\lambda}, \hat{x}, \hat{x}_m$ and $\hat{f}$ that are applicable in both the positive and negative gap regimes and defined by

$$\hat{\lambda} = \frac{H^{\infty}}{\bar{R}}, \quad \hat{x} = \frac{X}{\bar{R}}, \quad \hat{x}_m = \frac{X_M}{\bar{R}}, \quad \hat{f} = \frac{W}{\mu \bar{U}}. \tag{3.1}$$

Figure 7 shows predictions for their variation with $H_0/\bar{R}$ when $\nu = 0.5$ for the various models. A large disparity is observed for negative gaps between results of the FSM and the CCM with $K' = E/L$. The modified spring constant $K' = 4 \times E/L$, introduced by Carvalho & Scriven (1995*b*), has the effect of making the results for $\hat{\lambda}$ and $\hat{f}$ in close agreement with the FSM over the whole range of $H_0/\bar{R}$. This approach fails, however, to accurately predict $\hat{x}_m$; the position of the meniscus is greatly underpredicted by the modified CCM, which represents a serious shortcoming of this model since an accurate prediction of $\hat{x}_m$ is essential for the purposes of developing a stability analysis.

Further evidence of the inability of Hookean models to effectively model an incompressible compliant layer can be obtained by considering the behaviour of a deformable roll pair as $\nu \to 0.5$. All the field variables undergo rapid change: the flow rate rapidly decreases and the meniscus location moves further downstream, see Young (1997). Thus, since $0.45 \leqslant \nu \leqslant 0.5$ for elastomers, a spring model that is calibrated for a given value of ν cannot give satisfactory results at a different value and therefore such a model could not cover the full range of elastomeric materials. Figure 8 shows that as ν increases the pressure increases throughout the contact region and there is increased swelling of the compliant layer on either side of the contact region – thus increasing the contact width (note that deformation profiles

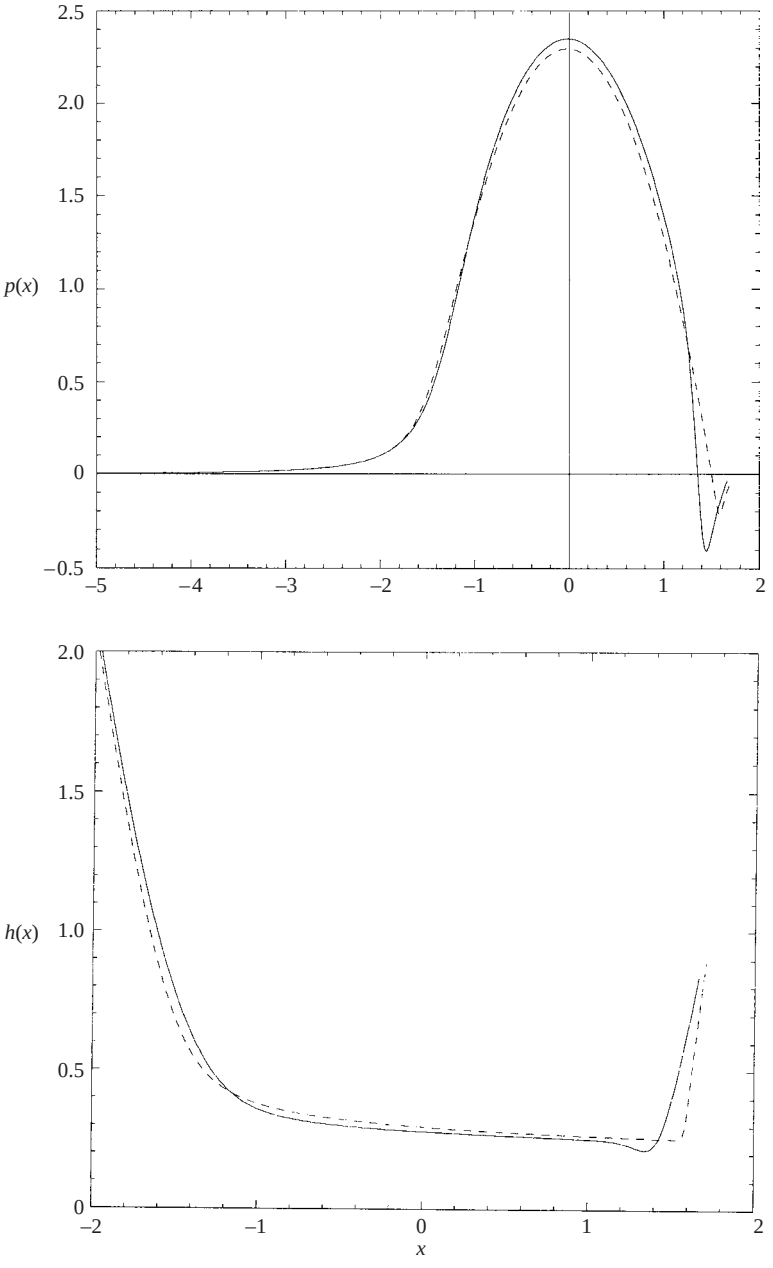

FIGURE 6. Profiles of $p(x)$ and $h(x)$ for the FSM (—) and CCM (– –) at $\nu = 0$; note the close agreement. $H_0/\bar{R} = -10^{-2}$, $E_S = 10^{-5}$, $Ca = 1$, $L/\bar{R} = 0.1$, $K' = E/L$.

have been terminated at x_m). Since Hookean 'spring' models assume that deformation $D(X)$ is proportional to local pressure $P(X)$ then it is clear from figure 8 that they are quite incapable of predicting layer swelling.

Hence we are left to conclude that for realistic operating conditions, the deformation of compliant layers ($\nu \approx 1/2$) cannot be modelled effectively by either Hookean models or the incompressible column model (ICM). In what follows the compliant layers are assumed to be incompressible, $\nu = 0.5$.

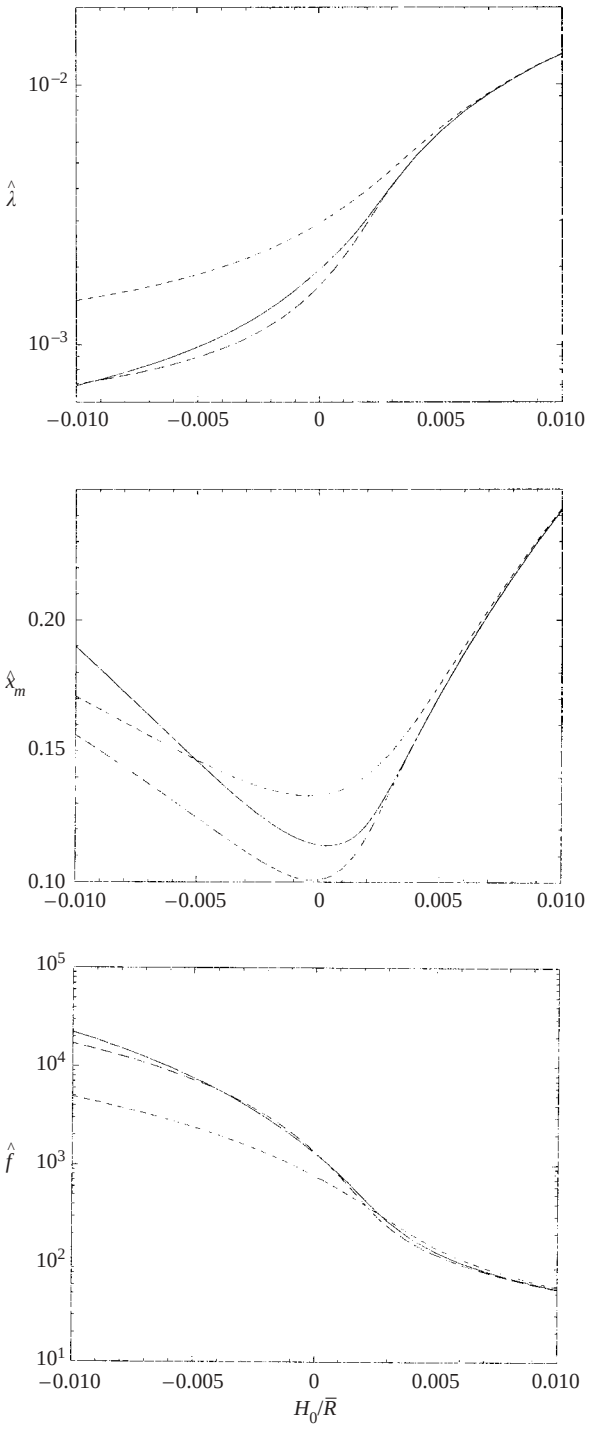

FIGURE 7. The variation of $\hat{\lambda}$, $\hat{x}_m$, and $\hat{f}$ with $H_0/\bar{R}$ for the CCM with $K' = E/L$ (- -) and $K' = 4 \times E/L$ (– –), and FSM (—). $L/\bar{R} = 0.1$, $E_S = 10^{-5}$, $Ca = 1$, $\nu = 0.5$.

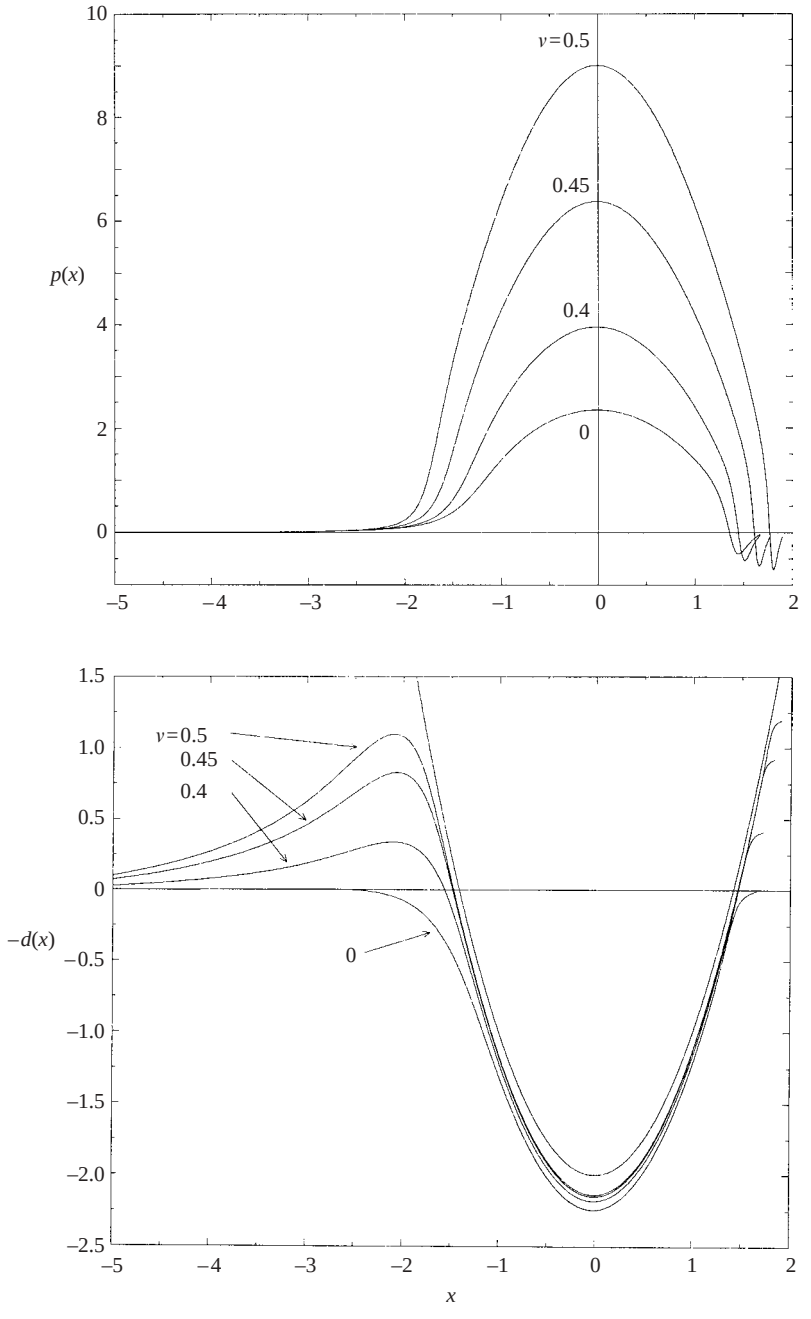

FIGURE 8. Profiles of $p(x)$ and $d(x)$ for the FSM for a range of ν; note the increase in maximum pressure, contact width, and layer swelling as $\nu \to 0.5$. $H_0/\bar{R} = -10^{-2}$, $E_S = 10^{-5}$, $Ca = 1$, $L/\bar{R} = 0.1$.

4. Equilibrium flow: lubricated contacts with an incompressible compliant layer

An equilibrium flow analysis is presented based on a soft EHL model which incorporates (i) the lubrication approximation for a thin film, (ii) film-splitting

boundary conditions, (iii) the FSM for the deformation of an incompressible layer ($\nu = 0.5$), and (iv) no viscoelastic effects, i.e. $T_\sigma = T_\epsilon = 0$.

Although results can be presented from the two different perspectives of fixed-gap operation and fixed-load operation, which are favoured by academic researchers and industrial operators respectively, here attention is restricted to fixed-gap operation. The distinction is made between positive- and negative-gap regimes, which essentially correspond to lightly loaded and heavily loaded regimes of EHL, and in each case the aim is to explore the effects due to layer thickness and elasticity.

It is possible to gain insight into the expected behaviour of the roll pair through a simple dimensional analysis. In the positive-gap/lightly loaded regime the pressure is assumed to be dominated by viscous forces:

$$P \sim \frac{\mu \bar{U}}{H_0} \left(\frac{\bar{R}}{H_0} \right)^{1/2}, \tag{4.1}$$

whereas in the negative-gap/highly loaded regime the deformation scales with the extent of the interference:

$$D \sim H_0, \tag{4.2}$$

and in both the positive- and negative-gap regimes the strain in the compliant layer is balanced with the stress:

$$\frac{D}{L} \sim \frac{P}{E}. \tag{4.3}$$

Thus in each regime either the scale for D or P is given and the stress–strain balance provides the remaining scale. This last balance suggests that L and E^{-1} may have the same effect. A scale for the dimensional flux, Q, in the negative-gap/highly loaded regime can be obtained by assuming that through the contact region the film thickness, H, is almost constant, and therefore balancing the pressure gradient ($\sim H_0 E / L\sqrt{H_0 \bar{R}}$) and the viscous stress ($\sim \mu \bar{U}/H^2$) gives

$$Q \sim UH \sim UR \left(\frac{\mu \bar{U}}{E \bar{R}} \right)^{1/2} \left(\frac{L}{\bar{R}} \right)^{1/2} \left(\frac{\bar{R}}{H_0} \right)^{1/4}. \tag{4.4}$$

Thus it appears that L and E^{-1} may have similar effects on the flux in this regime. The physical basis for the apparent similarity between E_S (or equivalently E^{-1}) and L via (4.3) is straightforward; it is simply that to make a given indentation requires a higher load if the compliant layer is made harder (increasing E) or shallower (decreasing L). One aim of the investigation is to determine the effect of L and E_S on the physical variables P, D, Q and X_M.

4.1. *Fixed-gap operation*

Solutions are generated for the parameter range

$$\frac{\mu \bar{U}}{E \bar{R}} \in [10^{-5}, 10^{-7}], \quad \frac{H_0}{\bar{R}} \in [-10^{-2}, 10^{-2}],$$

with $Ca = 1$, PH boundary conditions and $\nu = 0.5$. Results are expressed in terms of the modified non-dimensional variables $\hat{\lambda}$, $\hat{x}$, $\hat{x}_m$ and $\hat{f}$, defined by (3.1). Typical solution curves of pressure and gap thickness for both positive- and negative-gap regimes are displayed in figures 9 and 10. These are well-known results in elastohydrodynamic lubrication (Dowson & Higginson 1966); they illustrate that the effect of the compliant layer is to change the gap width near $X = 0$ from parabolic to locally linear with the slope tending to zero as the gap becomes increasingly negative (or the load increases). The variation of flow rate $\hat{\lambda}$ and meniscus location $\hat{x}_m$ with

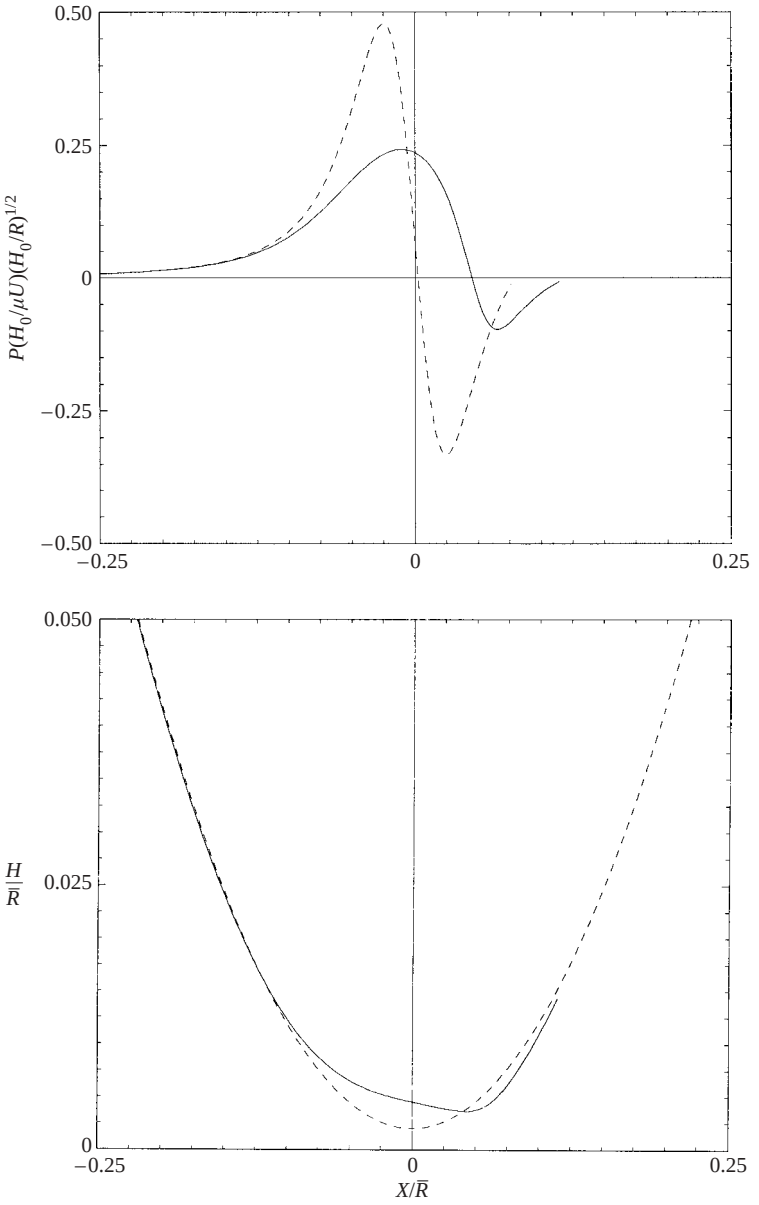

FIGURE 9. Profiles of pressure and gap width for a positive gap, using the FSM. Rigid roll asymptotes are also shown (- -). $\nu = 0.5$, $H_0/\bar{R} = 10^{-3}$, $E_S = 10^{-5}$, $Ca = 1$, $L/\bar{R} = 0.1$.

$H_0/\bar{R}$ is shown in figures 12 and 13 (for fixed $L/\bar{R}$ and E_S respectively) which also include the rigid roll and dry contact asymptotes for comparison.

4.1.1. *The positive-gap regime*

The effect of layer deformation for a positive gap, figure 9, is to modify $H(X)$ close to $X = 0$ so that the gap assumes a characteristic, almost linear, convergent film profile (see also Hooke 1986). The main effect on the pressure curve is observed to be a reduction in the magnitude of gradients and the maximum/minimum pressures.

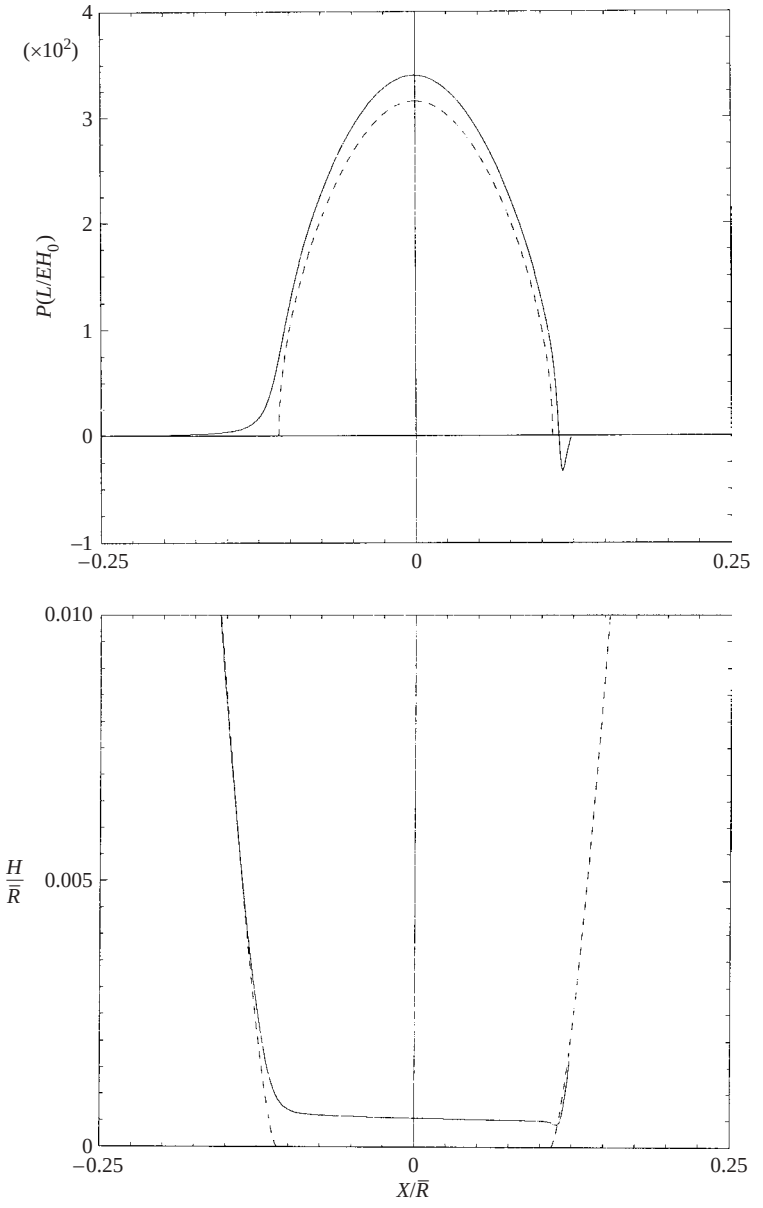

FIGURE 10. Profiles of pressure and gap width for a negative gap, using the FSM. Dry contact asymptotes are also shown (- -). $\nu = 0.5$, $H_0/\bar{R} = -5 \times 10^{-3}$, $E_S = 10^{-6}$, $Ca = 1$, $L/\bar{R} = 0.1$.

Varying the layer properties (layer thickness and elasticity) affects deformations to the compliant layer and consequently $\hat{\lambda}$ and $\hat{x}_m$. Intuitively we would expect elastic deformations to increase by using either a softer layer of material or a thicker one. It can be shown that, for positive gaps, deformations do increase with increasing L, see figure 11, and with increasing E_S (decreasing E). Figures 12 and 13 show that the behaviour of $\hat{\lambda}$ and $\hat{x}_m$ at large $H_0/\bar{R}$ is similar to that for fixed-gap rigid roll coating, with both decreasing as $H_0/\bar{R}$ is reduced. Furthermore, for a constant gap $H_0/\bar{R}$, both $\hat{\lambda}$ and $\hat{x}_m$ are seen to increase with E_S and with L. Hence one may conclude

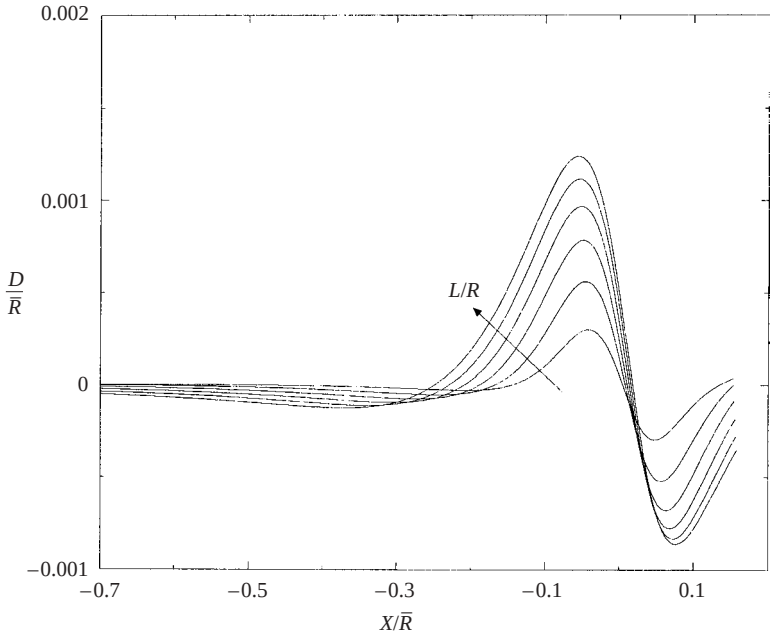

FIGURE 11. Deformation profiles. $H_0/\bar{R} = 4 \times 10^{-3}$, $Ca = 1$, $E_S = 10^{-5}$, $0.05 \leqslant L/\bar{R} \leqslant 0.2$, PH boundary conditions.

that, throughout the positive-gap regime, E_S and L have the same effect on layer deformation and on the system parameters $\hat{\lambda}$ and $\hat{x}_m$.

As a means of achieving very small flow rates the positive-gap rigid roll regime ceases to be practical due to the dual requirements of stiff rolls and a very small roll clearance. If ϵ is the total radial runout of the roll pair, then roll clash is avoided if

$$\frac{\varepsilon}{\bar{R}} \ll \frac{H_0}{\bar{R}}.$$

Typically $\varepsilon/\bar{R} \in [10^{-4}, 10^{-5}]$, and so rigid rolls are restricted to $H_0/\bar{R} > 10^{-4}$. This defines a minimum film thickness for fixed-gap rigid roll coating, below which deformable rolls come into their own.

4.1.2. *The negative-gap regime*

For negative gaps, figure 10, the gap thickness is small, convergent and yet almost constant throughout the contact region. Hence the pressure in this region has a similar profile to the dry-contact Hertzian asymptote together with an inlet pressure sweep and a sub-ambient loop just upstream of $\hat{x}_m$ – arising respectively due to the presence of a flooded inlet and film-splitting boundary conditions.

In the contact region, the rigid roll acts as an indentor, the degree of indentation is of $O(H_0)$ and both layer thickness, L, and E_S have little effect on the elastic deformations within the contact region. They do, however, significantly affect the pressure where the profile remains similar and close to the dry contact case. Numerical results confirm that the maximum pressure decreases with L and also E_S (figure 14) as suggested via relation (4.3).

At $X = 0$, figures 10 and 14 show that $\mathrm{d}P/\mathrm{d}X \approx 0$ and the fluid velocity has, therefore, only a Couette component. Hence flow rate is given by $\hat{\lambda} = H^{\infty}/\bar{R} \simeq H(0)/2\bar{R}$,

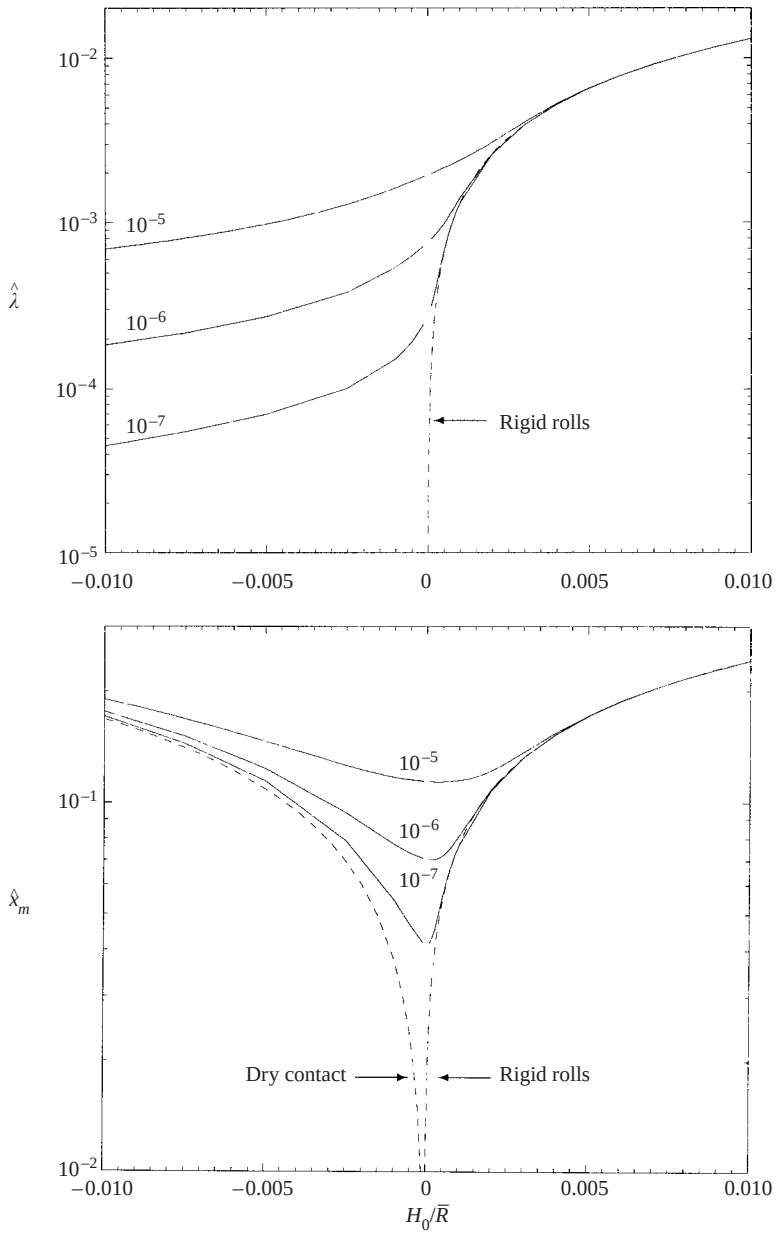

FIGURE 12. The variation of $\hat{\lambda}$ and $\hat{x}_m$ with $H_0/\bar{R}$, with $L/\bar{R} = 0.1$ fixed. The rigid roll ($E_S = 0$) (- -) and a highly loaded ($E_S = 10^{-7}$) asymptote are also shown. $E_S = 0, 10^{-7}, 10^{-6}$ and 10^{-5}; $Ca = 1$, PH boundary conditions.

which will diminish as gap thickness is reduced when the magnitude of $H_0/\bar{R}$ (load) is increased, see (4.4). This is confirmed in figure 12 which shows that thinner films can be generated than is practically feasible with a positive gap. Figure 12 also shows that as $\hat{\lambda}$ decreases the sensitivity of $\hat{\lambda}$ to $H_0/\bar{R}$ also decreases, thus giving a more robust production process than fixed-gap rigid roll coating in the sense that any deviation from the desired value of $H_0/\bar{R}$ has a small effect on $\hat{\lambda}$. In addition

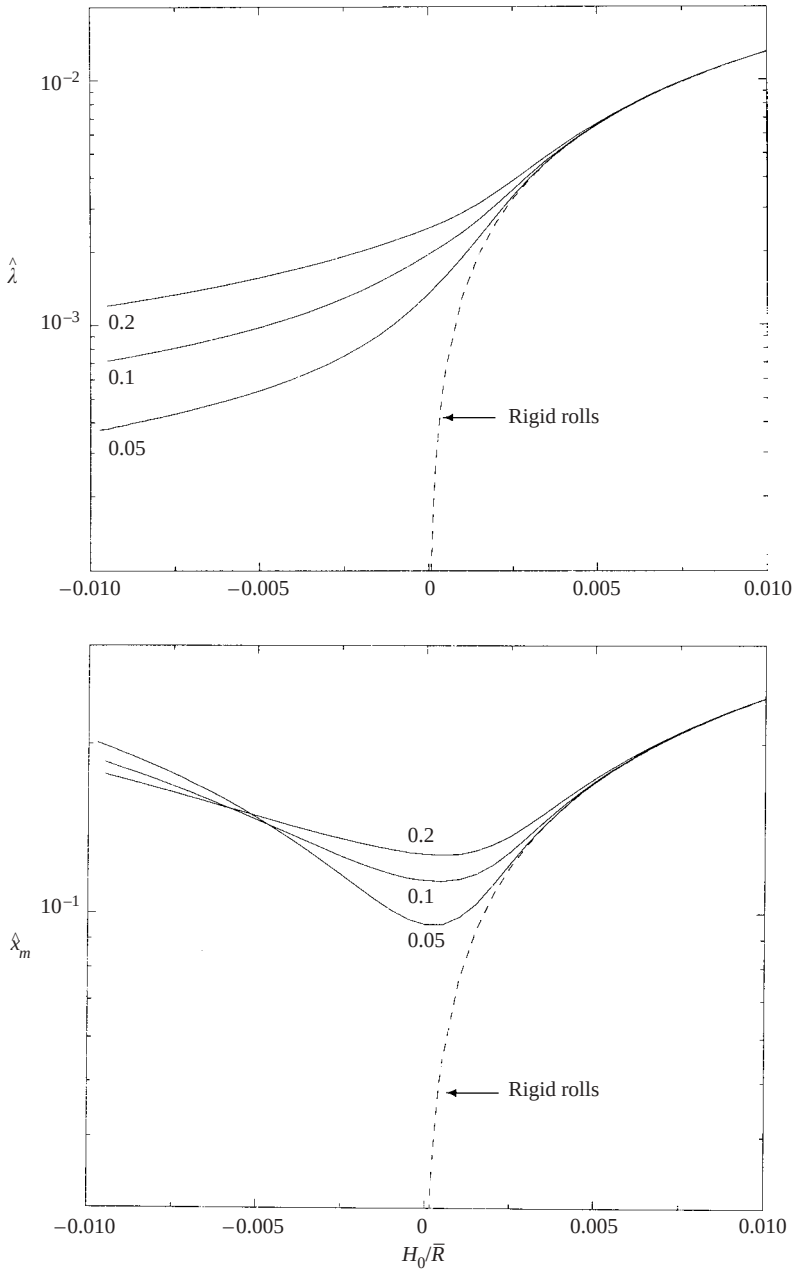

FIGURE 13. The variation of $\hat{\lambda}$ and $\hat{x}_m$ with $H_0/\bar{R}$, with $E_S = 10^{-5}$ fixed. The rigid roll asymptote corresponding to $E_S = 0$ is also shown (- -). $L/\bar{R} = 0.05, 0.1, 0.2$; $Ca = 1$, PH boundary conditions.

figures 12 and 13 show that E_S and L have the same effect on flow rate as for positive gaps.

As the coating regime changes from postive to negative gap, the location of the meniscus begins to move away from the nip, as shown in figures 12 and 13. This increase in $\hat{x}_m$ corresponds to an increase in nominal dry-contact width, $A^* =$

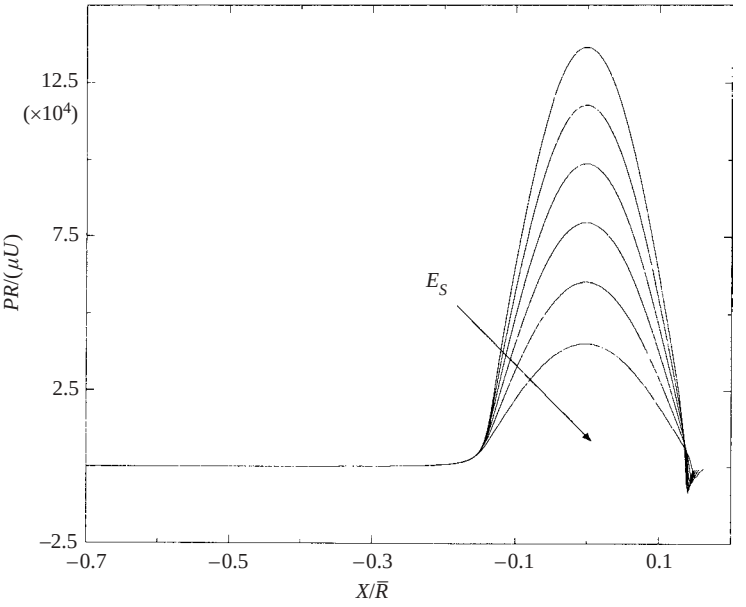

FIGURE 14. Pressure profiles. $H_0/\bar{R} = -7.5 \times 10^{-3}$, $Ca = 1$, PH boundary conditions.

$(2H_0\bar{R})^{1/2}$. The equivalent dry-contact width, $A/\bar{R}$, is also included and is approached as $H_0/\bar{R}$ is increased in magnitude.

The overall effects of E_S and $L/\bar{R}$ on $\hat{x}_m$ are clearly different. Figure 12 shows that, for a given $L/\bar{R}$, $\hat{x}_m$ increases with E_S whereas figure 13 indicates that, for a given E_S, $\hat{x}_m$ increases with $L/\bar{R}$ for 'small negative gaps' and decreases with $L/\bar{R}$ for 'large negative gaps'. These effects cannot be explained on the basis of earlier scaling arguments; rather it is necessary to examine 'layer swelling' at the edge of the contact region as shown in figure 8. The reader will note that it is essential to predict $\hat{x}_m$ accurately in order to subsequently analyse the stability of the liquid film/meniscus.

4.1.3. *Layer swelling at the edge of the contact region*

For negative gaps figures 12 and 13 reveal the different effects of elasticity E_S and layer thickness $L/\bar{R}$ on $\hat{x}_m$. In the former case $\hat{x}_m$ increases with E_S whereas in the latter $\hat{x}_m$ may move either towards or away from the nip as $L/\bar{R}$ increases, depending on the magnitude of $H_0/\bar{R}$. This behaviour is more clearly illustrated by selecting particular values of $H_0/\bar{R}$ ($H_0/\bar{R} = -2.0 \times 10^{-3}$, -5×10^{-3} and 7.5×10^{-3}) and plotting the variation of $\hat{x}_m$ with E_S ($L/\bar{R}$ fixed) and with $L/\bar{R}$ (E_S fixed). Figure 15 shows $\hat{x}_m$ increasing with E_S in each case whereas it shows $\hat{x}_m$ increasing with $L/\bar{R}$, for $H_0/\bar{R} = -2.0 \times 10^{-3}$, decreasing with $L/\bar{R}$, for $H_0/\bar{R} = -7.5 \times 10^{-3}$, and remaining almost constant for $H_0/\bar{R} = -5.0 \times 10^{-3}$.

The key to explaining the different effects of E_S and $L/\bar{R}$ on $\hat{x}_m$ is to first consider their effect on $D(X_M)/\bar{R}$, that is on layer swelling at the edge of the contact region. Figure 16 reveals that, for each of the three values of $H_0/\bar{R}$, $D(X_M)/\bar{R}$ shows little variation with E_S. However, for the same three values of $H_0/\bar{R}$, $D(X_M)/\bar{R}$ increases with $L/\bar{R}$. Hence $L/\bar{R}$ has significantly more effect on layer swelling than does E_S.

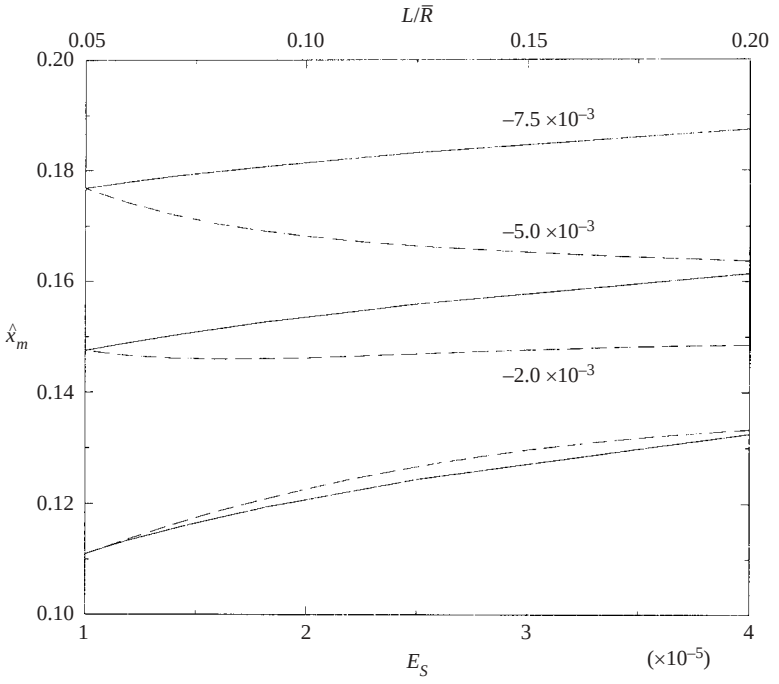

FIGURE 15. Variation of meniscus position with both E_S ($L/\bar{R} = 0.1$) (—) and $L/\bar{R}$ ($E_S = 10^{-5}$) (- - -) for three values of $H_0/\bar{R}$: -2.0×10^{-3}, -5.0×10^{-3} and -7.5×10^{-3}; $Ca = 1$, PH boundary conditions.

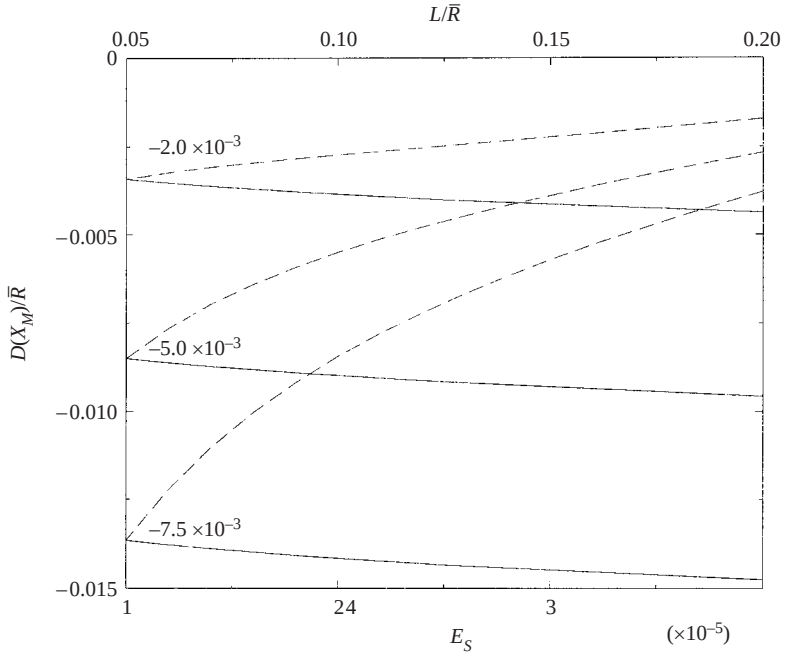

FIGURE 16. Variation of layer deformation at the meniscus with both E_S ($L/\bar{R} = 0.1$) (—) and $L/\bar{R}$ ($E_S = 10^{-5}$) (- - -) for three values of $H_0/\bar{R}$: -2.0×10^{-3}, -5.0×10^{-3} and -7.5×10^{-3}; $Ca = 1$, PH boundary conditions.

The behaviour of $\hat{x}_m$ in figure 15 can now be explained by referring to two expressions for the gap thickness at $\hat{x}_m$,

$$H(X_M) = 2H_0 + D(X_M) + \frac{X_M^2}{\bar{R}}, \tag{4.5}$$

and

$$H(X_M) = \frac{H^\infty}{\beta}. \tag{4.6}$$

For negative gaps with $\beta =$ constant and $H_0 =$ constant, if E_S or $L/\bar{R}$ are increased then flow rate, H^∞, increases (figures 12 and 13) as does $H(X_M)$ via (4.6). In particular:

(i) If E_S increases, $D(X_M)$ remains effectively constant – see figure 16 – and so via (4.5) it follows that $\hat{x}_m$ must increase – see figure 15.

(ii) If $L/\bar{R}$ increases, $D(X_M)/\bar{R}$ increases (becomes less negative) and it is precisely this behaviour of $D(X_M)/\bar{R}$ that determines the behaviour of $\hat{x}_m$:

(*a*) when $H_0/\bar{R} = -2 \times 10^{-3}$ the increase in $D(X_M)/\bar{R}$ is relatively small and so X_M must increase to ensure that $H(X_M)$ increases in accordance with (4.6);

(*b*) when $H_0/\bar{R} = -7.5 \times 10^{-3}$ the increase in $D(X_M)/\bar{R}$ is relatively large; in fact 'too large' so that x_m must decrease for $H(X_M)$ to increase in accordance with (4.6);

(*c*) when $H_0/\bar{R} = -5 \times 10^{-3}$ the increase in $D(X_M)/\bar{R}$ appears to be just sufficient for $H(X_M)$ to increase in accordance with (4.6) and as a consequence $\hat{x}_m$ remains almost constant.

4.1.4. *The sub-ambient pressure loop and the effect of the compliant layer on stability; the effect of Ca*

The sub-ambient pressure loop is re-displayed in figure 17, where the variation of $\hat{x}_m$, $\hat{p}(\hat{x}_m)$, and $\mathrm{d}\hat{p}(\hat{x}_m)/\mathrm{d}\hat{x}$ with $H_0/\bar{R}$ is more clear, with $\hat{p} = PL/E\bar{R}$. An important feature is the locus of the meniscus as $H_0/\bar{R}$ is decreased (increasing $\hat{f}$). The meniscus first moves in towards the nip, reaching its minimum position around the transition between positive- and negative-gap regimes, thereafter moving out as the effective Hertzian half-contact width increases. As $H_0/\bar{R}$ is decreased, $\hat{\lambda}$ reduces (see figures 12 and 13) and $\hat{p}(\hat{x}_m)$ and $\mathrm{d}p(\hat{x}_m)/\mathrm{d}\hat{x}$ vary according to the relationships

$$\hat{p}(\hat{x}_m) \sim -\frac{1}{\hat{\lambda}}, \quad \left.\frac{\mathrm{d}\hat{p}}{\mathrm{d}\hat{x}}\right|_{\hat{x}_m} \sim \frac{1}{\hat{\lambda}^2}, \tag{4.7}$$

which follow from (2.10) and (2.16) respectively. Therefore, $\hat{p}(\hat{x}_m)$ becomes more negative with decreasing (more negative) $H_0/\bar{R}$, whilst $\mathrm{d}\hat{p}(\hat{x}_m)/\mathrm{d}\hat{x}$ increases. The pressure gradient remains positive for both positive and negative gaps and therefore has a destabilizing effect on the meniscus that gives rise to the three-dimensional ribbing instability.

To understand the influence that layer deformation has on stability one must examine the consequences of the change in geometry (inter-roll film thickness) close to X_M where

$$\left.\frac{\mathrm{d}H}{\mathrm{d}X}\right|_{X_M} = 2X_M + \left.\frac{\mathrm{d}D}{\mathrm{d}X}\right|_{X_M}. \tag{4.8}$$

Since an increase in $\mathrm{d}H/\mathrm{d}X|_{X_M}$ stabilizes the film-splitting process (Pitts & Greiller 1961 and Savage 1977), it follows that both X_M and $\mathrm{d}D/\mathrm{d}X|_{X_M}$ will contribute to stability. In the vicinity of the meniscus there is layer swelling due to the incompressiblity of the compliant layer and for light to moderate loads (positive

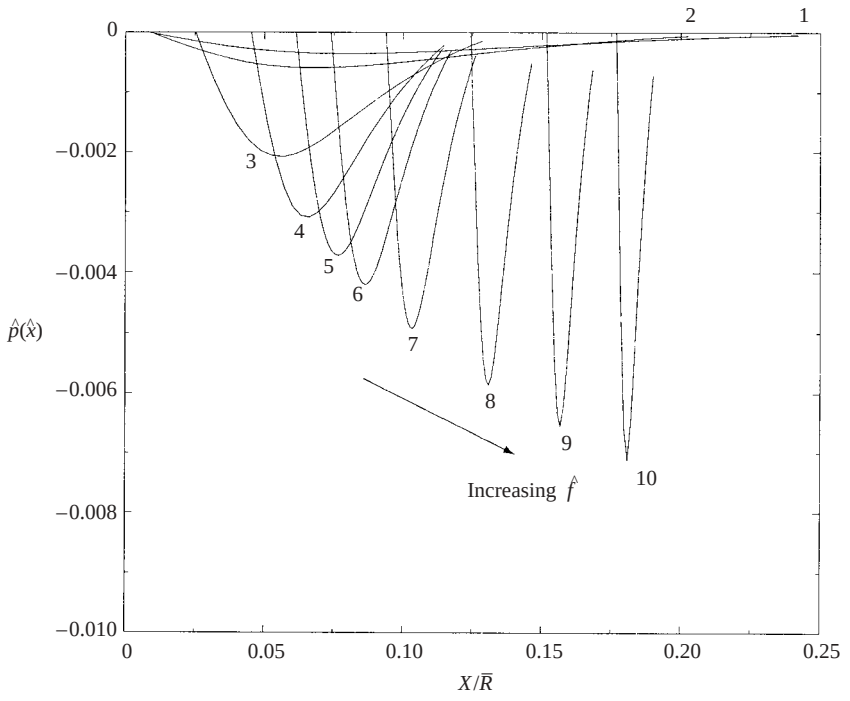

FIGURE 17. The variation of $\hat{p}(\hat{x})$ local to x_m as $\hat{f}$ is increased. $L/\bar{R} = 0.1$, $E_S = 10^{-5}$, $\nu = 0.5$, $Ca = 1$.

gaps), $\mathrm{d}D/\mathrm{d}X|_{X_M} > 0$ as illustrated in figure 11. This is the reason why compliant layers have a stabilizing effect in deformable roll coating with positive gaps.

For high loads (negative gaps) the situation is less clear since it can be shown that $\mathrm{d}D/\mathrm{d}X|_{X_M}$ is now negative thus providing a destabilizing influence. Nevertheless, as $H_0/\bar{R}$ becomes more negative, there is the possibility for an unstable film-splitting process to restabilize itself, depending on the competition between opposing effects due to pressure gradient and $T\mathrm{d}H/\mathrm{d}X|_{X_M}$. Clearly, only a full stability analysis will reveal the particular effects due to $L/\bar{R}$ and E_S on the stability of deformable roll coating with negative gaps.

When the PH conditions are applied in fixed-gap rigid roll coating, usually for flooded inlets and in the range $Ca > 1$, $\hat{x}_m$ and $\hat{\lambda}$ are virtually independent of Ca. The same is true for deformable roll coating with large positive gaps yet as $H_0/\bar{R}$ is decreased and eventually becomes negative the behaviour depends upon the manner in which Ca is varied, that is whether the viscosity, speed or surface tension is varied. If Ca is varied with E_S held constant (i.e. variable surface tension) then the fixed-gap rigid roll result still stands. However, if Ca is varied with Ca/E_S held constant (i.e. variable viscosity or roll speed) then $\hat{\lambda}$ and $\hat{x}_m$ alter significantly. Therefore, the interaction of viscous and elastic forces enables the viscosity and roll speed to play an important role in determining both the film thickness and meniscus location.

4.2. *Experimental validation*

Unfortunately, insufficient information concerning the thickness and compressibility of the deformable layer generally precludes any comprehensive comparison between theoretical predictions and available experimental data. An exception is the work of

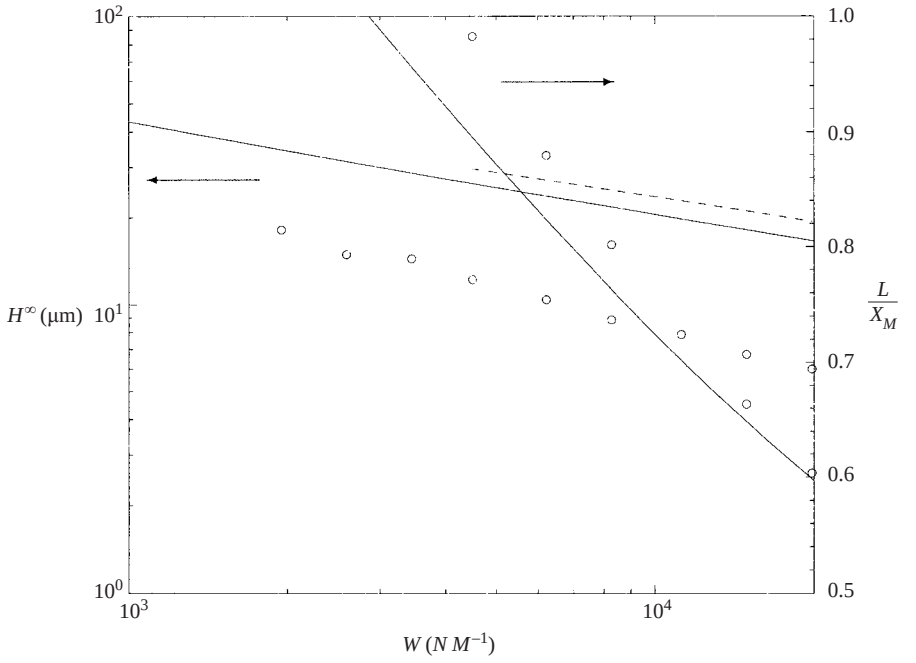

FIGURE 18. A comparison of mathematically predicted (—) and experimentally measured (○) H^∞ and L/X_M for a range of loads with $H_0/\bar{R} \in [-10^{-3}, -10^{-2}]$, $E_S = 0.576 \times 10^{-6}$, $Ca = 0.1$, $\nu = 0.5$, and $L/\bar{R} = 0.102$, for which $\alpha \in [\sqrt{2}, 1]$. Predictions due to Jaffar (1990) are also shown (- -).

Cohu & Magnin (1995), in which coated film thickness was measured for a range of applied loads with all relevant information recorded to enable a comparison with predictions from the purely elastic FSM. As applied load is varied both the predicted and measured values of coated film thickness, H^∞, are compared in figure 18, along with values for L/X_M, which is proportional to the strip number, $\alpha = L/\bar{R} \times (H_0/\bar{R})^{-1/2}$. Cohu & Magnin's data are for $L/X_M < 1$, i.e. when the compliant layer deforms as a thin strip and the sensitivity of H^∞ was observed to increase. Predicted and measured values of L/X_M are seen to be in good agreement, especially for high loads, whereas predictions for H^∞ exceed the experimental results by a factor of two. Possible reasons for this discrepancy are experimental error due to the accuracy of scraping when measuring a coated film thickness of approximately 10 μm or viscoelastic effects in the deformable layer.

Cohu & Magnin state that experimental error could be as much as 30% for thin films but this alone cannot explain the difference between theory and experiment. Here, viscoelastic effects are examined by setting T_σ and T_ϵ in (2.17)–(2.19) to non-zero values. To accurately model an elastomer a spectrum of retardation and relaxation times should be used but as no data exist for the viscoelastic properties (i.e. shear modulus G' and loss modulus G'') of the elastomers used in the experiments, single values of T_σ and T_ϵ were selected (giving a modified Deborah number $De(H_0/\bar{R})^{1/2} = 3 \times 10^{-2}$ and $T_\epsilon/T_\sigma = 10^2$) with the aim of investigating what effect the inclusion of the viscoelastic terms has on the predictions of the FSM. Figure 19 shows, for typical operating conditions, the variation of the flux and meniscus position with load as predicted by the FSM, both with and without the viscoelastic terms included. It is

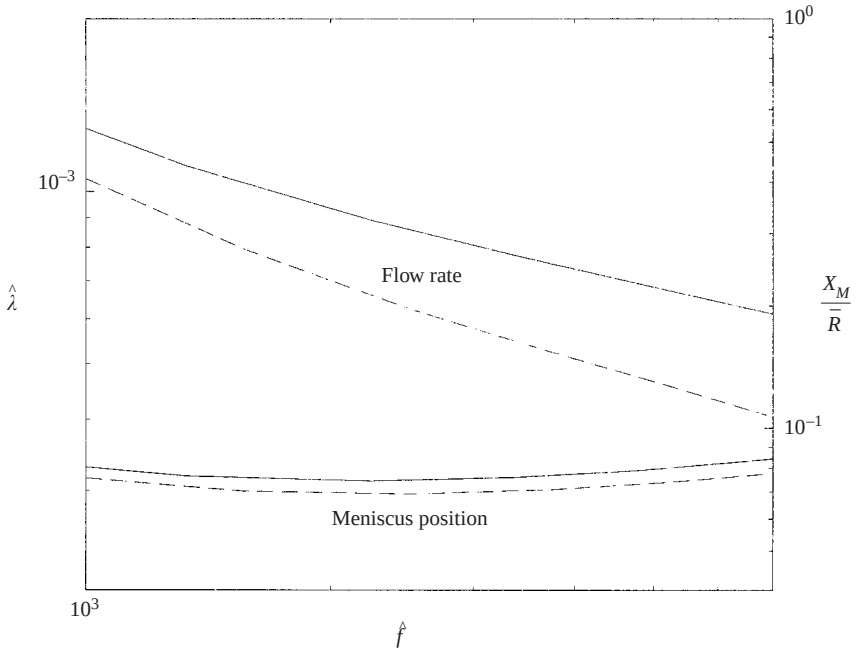

FIGURE 19. Variation of flux and flow rate against load with (- -) and without (—) viscoelastic terms. $L/\bar{R} = 0.2$, $E_S = 10^{-6}$ and $Ca = 1$.

clear that the introduction of these terms has a dramatic effect on the magnitude of the flux, with the reduction being of the order of 60% for high loads, yet the effect on X_M is much less pronounced, the maximum difference being 6%. It is therefore apparent that viscoelastic effects could be responsible for the discrepancy between theoretical predictions and experimental measurements of the flux and this is an area which merits further investigation.

REFERENCES

ALEKSANDROV, V. M. 1962 Contact problem of a stamp on an elastic layer: English translation. *Prikl. Mat. Mekh.* **27**, 1490.

BENJAMIN, D. F. & SCRIVEN, L. E. 1992 Coating flows analysed by form and function. *Ind. Coating Res.* **2**, 1–31.

BENKREIRA, H., EDWARDS, M. F. & WILKINSON, W. L. 1981 A semi-empirical model of the forward roll coating flow of Newtonian fluids. *Chem. Engng Sci.* **36**, 423–427.

BENTALL, R. H. & JOHNSON, K. L. 1968 An elastic strip in plane rolling contact. *Intl J. Mech. Sci.* **10**, 637–663.

BOHAN, M. F. J., LIM, C. H., KOROCHKINA, T. V., CLAYPOLE, T. C., GETHIN, D. T. & ROYLANCE, B. J. 1997 An investigation of the hydrodynamic and mechanical behaviour of a soft nip rolling contact. *J. Engng Trib.* **211**, No. J1, 37–49.

CARVALHO, M. S 1999 Non-linear elastoviscous model of deformable roll cover. In *Advances in Coating and Drying of Thin Films: Proc. Third European Symp.* (ed. F. Durst & H. Raszillier), pp. 265–270. Shaker.

CARVALHO, M. S. & SCRIVEN, L. E. 1994 Effect of deformable roll covering on roll coating. *TAPPI J.* **77** (5), 201.

CARVALHO, M. S. & SCRIVEN, L. E. 1995*a* Deformable roll coating: Analysis of ribbing instability and its delay. In *The Mechanics of Thin Film Coating: Proc. First European Symp.* (ed. P. H. Gaskell, M. D. Savage & J. L. Summers), pp. 75–84. World Scientific.

Carvalho, M. S. & Scriven, L. E. 1995*b* Deformable roll coating: Modeling of steady flow in gaps and nips. In *The Mechanics of Thin Film Coating: Proc. First European Symp.* (ed. P. H. Gaskell, M. D. Savage & J. L. Summers), pp. 221–230. World Scientific.

Carvalho, M. S. & Scriven, L. E. 1996 Capillary and viscoelastic effects on elastohydrodynamic lubrication in roller nips. *Trans. ASME: J. Tribol.* **118**, 872–879.

Carvalho, M. S. & Scriven, L. E. 1997*a* Deformable roll coating: steady state and linear perturbation analysis. *J. Fluid Mech.* **339**, 143–172.

Carvalho, M. S. & Scriven, L. E. 1997*b* Flows in forward deformable roll coating gaps: comparison between spring and plane-strain models of roll cover. *J. Comput. Phys.* **138**, 449–479.

Carvalho, M. S. & Scriven, L. E. 1999 Three-dimensional stability analysis of free surface flows: applications to forward deformable roll coating. *J. Comput. Phys.* **151**, 534–562.

Cohu, O. & Magnin, A. 1995 Experimental investigations on roll coating with deformable rolls. In *The Mechanics of Thin Film Coating: Proc. First European Symp.* (ed. P. H. Gaskell, M. D. Savage & J. L. Summers), pp. 179–188. World Scientific.

Cohu, O. & Magnin, A. 1997 Forward roll coating of Newtonian fluids with deformable rolls: an experimental investigation. *Chem. Engng Sci.* **52**, 1339–1347.

Coyle, D. J. 1988 Forward roll coating with deformable rolls: A simple one dimensional elasto-hydrodynamic model. *Chem. Engng Sci.* **43**, 2673–2684.

Coyle, D. J. 1997 Knife and roll coating. In *Liquid Film Coating* (ed. S. F. Kistler & P. M. Schweizer), pp. 539–571. Chapman and Hall.

Coyle, D. J., Macosko, C. W. & Scriven, L. E. 1986 Film-splitting flows in forward roll coating. *J. Fluid Mech.* **171**, 183–207.

Coyle, D. J., Macosko, C. W. & Scriven, L. E. 1990*a* The fluid dynamics of reverse roll coating. *AIChE J.* **36**, No. 2, 161–174.

Coyle, D. J., Macosko, C. W. & Scriven, L. E. 1990*b* A simple model of reverse roll coating. *Ind. Engng Chem. Res.* **29**, 1416–1419.

Decre, M., Gailly, E. & Buchlin, J. M. 1995 Meniscus shape experiments in forward roll coating. *Phys. Fluids* **7**, 458–467.

Dowson, D. & Higginson, G. R. 1966 *Elasto-hydrodynamic Lubrication.* Pergamon.

Dowson, D. & Whitaker, A. V. 1965 The iso-thermal lubrication of cylinders. *ASLE Trans.* **8**, 224–234.

Elsharkawy, A. A. & Hamrock, B. J. 1995 Elasto-hydrodynamic lubrication of elastomeric covered surfaces in line contact. *Proc. Inst. Mech. Engrs* **209**, 119–130.

Gaskell, P. H., Innes, G. E. & Savage, M. D. 1998 An experimental investigation of meniscus roll coating. *J. Fluid Mech.* **355**, 17–44.

Gaskell, P. H., Savage, M. D., Summers, J. L. & Thompson, H. M. 1995 Modelling and analysis of meniscus roll coating. *J. Fluid Mech.* **298**, 113–137.

Gaskell, P. H., Savage, M. D. & Thompson, H. M. 1998 Stagnation-saddle points and flow patterns in Stokes flow between contra-rotating cylinders. *J. Fluid Mech.* **370**, 221–247.

Goryacheva, I. G. 1998 *Contact Mechanics in Tribology*. Kluwer.

Gostling, M. J. 2002 Instabilities in rigid and deformable roll coating. PhD thesis, University of Leeds.

Greener, J. & Middleman, S. 1975 A theory of roll coating of viscous and viscoelastic fluids. *Polymer Engng and Sci.* **15**, 1–10

Hall, R. W. & Savage, M. D. 1988*a* Two-dimensional elastohydrodynamic lubrication. 1. The associated dry contact problem *Proc. Inst. Mech. Engrs* C **202**, No. 5, 347–353

Hall, R. W. & Savage, M. D. 1988*b* Two-dimensional elastohydrodynamic lubrication. 2. Solution of the line contact problem. *Proc. Inst. Mech. Engrs* C **202**, No. 5, 354–360.

Hamrock, B. J. 1966 *Elasto-hydrodynamic Lubrication.* Pergamon.

Herrebrugh, K. 1968 Solving the incompressible and isothermal problem in elastohydrodynamics through an integral equation. *Trans. ASME: J. Lubric. Tech.* **90**, 262–270.

Ho, W. S. & Holland, F. A. 1978 Between rolls metering coating technique: A theoretical and experimental study. *TAPPI J.* **61**, No. 2, 53–56.

Hooke, C. J. 1986 Elasto-hydrodynamic lubrication of a cylinder on a elastomeric layer. *Wear* **111**, 83–99.

Hooke, C. J. & O'Donoghue, J. P. 1972 Elasto-hydrodynamic lubrication of soft, highly deformed contacts. *J. Mech. Engng Sci.* **14**, 34–48.

Hopkins, M. R. 1957 Viscous flow between rotating cylinders and a sheet moving between them. *Brit. J. Appl. Phys.* **8**, 442–444.

Houpert, L. D. & Hamrock, B. J. 1986 Fast approach for calculating film thickness and pressure in elasto-hydrodynamically lubricated contacts at high loads. *Trans. ASME: J. Tribol.* **108**, 411–420.

Jaffar, M. J. 1990 Two-dimensional elasto-hydrodynamic lubrication of elastic strips. *Wear* **139**, 335–350.

Jaffar, M. J. & Savage, M. D. 1988 On the numerical solution of line contact problems involving bonded and unbonded strips. *J. Strain Anal.* **23**, 67–77.

Jin, Z. & Dowson, D. 1989 The influence of elastic deformation upon film thickness in lubricated bearings with low elastic modulus. In *Proc. Leeds–Lyon Symp.* (ed. C. M. Taylor & D. Dowson), pp. 263–269. Elsevier.

Johnson, K. L. 1970 Regimes of elasto-hydrodynamic lubrication. *J. Mech. Engng Sci.* **12**, 9–16.

Landau, L. & Levich, B. 1942 Dragging of a liquid be a moving plate. *Acta Physicochemia URSS* **17** (1–2), 42.

Malone, B. 1992 An experimental investigation of roll coating phenomena. PhD thesis, University of Leeds.

Meijers, P. 1968 The contact problem of a rigid cylinder on an elastic layer. *Appl. Sci. Res.* **18**, 353–382.

Myers, T. G., Savage, M. D. & Gaskell, P. H. 1994 The indentation of an elastic layer by a sharp punch. *J. Mech. Appl. Maths* **47**, 129–140.

Pitts, E. & Greiller, J. 1961 The flow of thin liquid films between rollers. *J. Fluid Mech.* **11**, 33–50.

Prandtl, L. 1904 Motion of fluids with very little viscosity. *Tech. Mem. Natl Adv. Comm.* **452**.

Ruschak, K. J. 1982 Boundary conditions at a liquid–air interface in lubrication flow. *J. Fluid Mech.* **119**, 107–120.

Ruschak, K. J. 1985 Coating flows. *Annu. Rev. Fluid Mech.* **17**, 65–89.

Savage, M. D. 1977 Cavitation in lubrication. Part 2. Analysis of wavy interfaces. *J. Fluid Mech.* **80**, 757–767.

Xue, Y. K., Gethin, D. T. & Lim, C. H. 1994 Numerical modelling of the contact between lithographic printing press rollers by soft EHL thory. *J. Engng Tribol.* **208**, 257–268.

Xue, Y. K., Gethin, D. T. & Lim, C. H. 1996 Elastohydrodynamic lubrication analysis of layered line contact by the boundary element method. *Intl J. Numer. Meth. Engng* **39**, 2531–2554.

Young, A. E. 1997 A theoretical and experimental investigation of deformable roll coating. PhD thesis, University of Leeds.